ACE2 Homo-dimerization, Human Genomic variants and Interaction of Host Proteins Explain High Population Specific Differences in Outcomes of COVID19

Swarkar Sharma[1*], Inderpal Singh[2†], Shazia Haider[3†], Md. Zubbair Malik[4†], Kalaiarasan Ponnusamy[5†], Ekta Rai[1]

1. Human Genetics Research Group, School of Biotechnology, Shri Mata Vaishno Devi University, Katra, Jammu and Kashmir, India.
2. Bioinfores Pvt. Ltd., R. S. Pura, Jammu, Jammu and Kashmir, India.
3. Department of Biotechnology, Jaypee Institute of Information Technology, Noida, Sector-62, Uttar Pradesh, India
4. School of Computational and Integrative Sciences, Jawaharlal Nehru University, New Delhi, India.
5. School of Biotechnology, Jawaharlal Nehru University, New Delhi, India.

† - All authors contributed Equally

Corresponding Author:
Dr. Swarkar Sharma
Coordinator, Human Genetics Research Group,
School of Biotechnology, Shri Mata Vaishno Devi University, Katra, J&K, India
Email: swarkar.sharma@smvdu.ac.in
Mobile: +91-9419955636; Ph: +91-1991-285535//285525 Ext. 2385

ABSTRACT

Severe acute respiratory syndrome coronavirus 2 (SARS-CoV-2) is a positive single stranded RNA virus that causes a highly contagious Corona Virus Disease (COVID19). Entry of SARS-CoV-2 in human cells depends on binding of the viral spike (S) proteins to cellular receptor Angiotensin-converting enzyme 2 (ACE2) and on S-protein priming by host cell serine protease TMPRSS2. Recently COVID19 has been declared pandemic by World Health Organization yet high differences in disease outcomes across countries have been seen. We provide evidences based on analyses of existing public datasets and by using various *in-silico* approaches to explain some of these as factors that may explain population level differences. One of the key factors might be entry of virus in host cells due to differential interaction of viral proteins with host cell proteins due to different genetic backgrounds. Based on our findings, we conclude that higher expression of *ACE2* facilitated by natural variations, acting as Expression quantitative trait loci (eQTLs) and with different frequencies in different populations, results in ACE2 homo-dimerization which is disadvantageous for TMPRSS2 mediated cleavage of ACE2 and becomes more difficult in presence of broad neutral amino acid transporter, B0AT1 (coded by *SLC6A19*), that usually does not express in Lungs. We also propose that the monomeric ACE2 has higher preferential binding with SARS-CoV-2 S-Protein vis-a-vis its dimerized counterpart. Further, eQTLs in *TMPRSS2* and natural structural variations in the gene may also result in differential outcomes towards priming of viral S-protein, a critical step for entry of Virus in host cells. In addition, we suggest some other potential key host genes like *ADAM17, RPS6, HNRNPA1, SUMO1, NACA, BTF3* and some other proteases as Cathepsins, which might have a critical role. Understanding these population specific differences may help in developing appropriate management strategies.

Introduction

The recent emergence of corona virus disease (COVID19) caused by severe acute respiratory syndrome (SARS) coronavirus 2 (SARS-CoV-2) has resulted in >3.5 Million infections and >240 thousands deaths worldwide so far, and the numbers are increasing exponentially [https://covid19.who.int/]. SARS-CoV-2 is reported to be originated in bats (Zhou, et al., 2020) and transmitted to humans via unknown intermediate host. However, its origin is still being questioned time and again. With the declaration of SARS-CoV-2 as pandemic by World Health Organisation (WHO), extensive research worldwide has been carried out. It has been established that Human ACE2 mediates SARS-CoV-2 entry into cells through its Spike (S) Protein which primarily makes entry to host body through respiratory tract with recent reporting of nasal epithelial cells as potential initial infection site (Sungnak, et al., 2020). ACE2 is functional receptor on human cells for this newly originated coronavirus (Walls, et al., 2020) with higher affinity then severe acute respiratory syndrome coronavirus (SARS-CoV) originated in 2002 (Wan, et al., 2020). However, no substantial evidence exists that higher expression of ACE2 is primarily associated with degree of infection (Kuster, et al., 2020). Additionally, COVID19 lethality is mostly driven by the extent of underlying lung injury whereas, a negative correlation has been reported between ACE2 expression and lung injury (Imai, et al., 2005) and recent report suggests inhibition of SARS-CoV-2 by human recombinant soluble (hrs) ACE2 (Monteil, et al., 2020), making it an interesting question to explore.

High differences in clinical outcomes across countries have been [https://covid19.who.int/] noted which demonstrate that neither all people who are exposed to SARS-CoV-2 develop infection nor all infected patients end up in severe respiratory illness (Guan, et al., 2020), and it cannot be explained by immunity alone (Shi, et al., 2020) . This results in hypothesis of differential genetic susceptibility to COVID19 and virulence of SARS-CoV-2 in different populations (Kaiser, 2020). Efforts are being made worldwide to gain a better understanding of this disease and hypothesis as complex as role of Bacillus Calmette–Guérin (BCG) vaccine, a vaccine primarily used against tuberculosis (TB), for reduced morbidity and mortality for COVID19 in human population (Miller, et al., 2020) are developing. Due to extensive contemporary research, evidences in favour (Stawiski, et al., 2020) as well as against (Cao, et al., 2020) the existence of SARS-CoV-2 S-protein binding-resistant ACE2 natural variants, in different populations, have been found recently. In addition, studies highlighting role of eQTLs in *ACE2* expression and resulting in potential differential COVID19 fatality (Cao, et al., 2020; Chen, et al., 2020) are pouring in. Where most of such studies are targeting only natural variations in ACE2 gene as SARS-CoV-2 differential susceptibility factor, recent evidences suggest that additional host proteins like cellular serine protease TMPRSS2 act as co-factors and are critical for efficient cellular infection by SARS-CoV-2 (Hoffmann, et al., 2020). Further, it is equally important to consider that rare functional variants, though may have consequences, yet may not explain large scale population level differential clinical outcomes.

This highlights the importance of identification of such other potential co-factors and underlying mechanisms these genes can play. At the same time, understanding correlations between these host proteins and their interactions with SARS-CoV-2 and ACE2 may explain many of the unanswered questions. Further evaluating these host genes, exploring natural occurring variants in these, their expression patterns may also shed some light on better understanding of differential susceptibility to COVID19 and virulence of SARS-CoV-2. In the present study, we have tried to exploit existing literature to understand mechanisms of correlations, of host genes, specifically associated with interactions related to ACE2 and some prominent viral proteins, using *in-silico* approaches and tried to understand these as factors explaining population level differences.

Methodology

As SARS-CoV-2 is primarily a respiratory pathogen, the present study was conducted to understand mechanisms of its entry to cells in lungs and we believe it can be extrapolated to other respiratory tract tissues to explore potential factors that may result in to differential outcomes in respiratory illness. To being with, we started with the most studied host protein ACE2 and tried to understand its interaction with SARS-CoV-2 S-Protein through Molecular Dynamics simulations, followed by adding other interacting proteins. We further added layers of other methods to have a better understanding of the potential causes and outcomes.

Molecular Dynamics (MD) Simulations

Recently submitted experimental structure 6M17.pdb of ACE2 dimer bound to two B0AT1 (coded by *SLC6A19*) and two receptor-binding domains (RBD) of S1of SARS-CoV-2 Spike protein (S-protein), with overall resolution of 2.90 Angstrom and SARS-CoV2 Spike Glycoprotein with RBD domain in Up conformation (6VSB.pdb) were downloaded from the Protein Data Bank for structural, visualization and dynamics analysis (Wrapp, et al., 2020; Yan and Zhang, 2020). This structure was corrected for missing amino acids, side chains, missing hydrogen atoms, correction of disulphide bonds etc., optimized for pKa corresponding to physiological pH 7.2 and energy minimized to correct steric clashes using the Protein Preparation Wizard of Schrodinger Maestro (Madhavi Sastry, et al., 2013). Predefined solvation model TIP3P was used and overall neutrality of the system was maintained by addition of Na+ and Cl- counter ions(Mark and Nilsson, 2001). Physiological salt concentration of 0.15 Molar was generated through addition of NaCl. Periodic boundary condition of 10 Angstrom was set using the System Builder Tool of Desmond software(2006). Total two MD simulations, each 10 nanosecond long, were conducted. In one of the simulation, six chains i.e. ACE2 dimer with each monomer bound to a B0AT1 and RBD domain was simulated and the resulting solvated system consisted of 424,847 atoms, while for other simulation monomeric ACE2 bound to viral RBD consisted of 174,900 atoms. Root mean square fluctuation (RMSF) and principal component analysis were done through R based BIO3D module (Grant, et al., 2006). MMGBSA free energy of binding between proteins was calculated through Prime Software of Schrodinger Suite (Jacobson, et al.,

2002). Structural visualizations and images were traced using pyMOL and VMD (Jacobson, et al., 2002) (Humphrey, et al., 1996).

Gene Expression in Alternate Transcripts and Regulation Analyses

Genotype-Tissue Expression (GTEx) portal at https://gtexportal.org/ was used to explore various gene expression. By Tissue, Multigene Query as well as transcript browser was used to understand expression of splice variants and exons in Lungs. eQTLs were viewed by GTEx IGV Browser as well as GTEx Locus Browser was used to plot gene specific eQTLs. eQTLs and other gene regulatory information, splice variants and ESTs were also explored through UCSC genome browser https://genome.ucsc.edu/ with build GRCh37/hg19. Table browser was used to interact various datasets to look for overlaps and filter outcomes. Retrieved information was saved in files as well as plotted on UCSC browser as custom tracks. Comparison of RNA expression and Protein expression, mainly in lungs, was done at The Human Protein Atlas (Uhlen, et al., 2015) at www.proteinatlas.org. HaploReg v4.1 (https://pubs.broadinstitute.org/mammals/haploreg/haploreg.php) was used to annotate effect of noncoding genome variants of regulation motifs.

Analyses of Allele frequencies distribution of Variants in different population Groups

Genetic data for global population groups was explored through the GnomAD portal at https://gnomad.broadinstitute.org/, as well as dbSNP database of NCBI at https://www.ncbi.nlm.nih.gov/snp. Gene specific SNPs data was also retrieved from 1000 genomes (1000G) Phase 3 data set available through https://www.ncbi.nlm.nih.gov/variation/tools/1000genomes as per Homo sapiens:GRCh37.p13 (GCF_000001405.25). Data for the population groups belonging to five super population groups [African (AFR), Ad mixed American (AMR), East Asian (EAS), European (EUR) and South Asian (SAS)] was analysed. The following sub population groups were studied. AFR: African Caribbeans in Barbados (ACB), Americans of African Ancestry in SW USA (ASW), Esan in Nigeria (ESN), Gambian in Western Divisions in the Gambia (GWD), Luhya in Webeye, Kenya (LWK), Mende in Sierra Leone (MSL), Yoruba in Ibadan, Nigeria (YRI). AMR: Colombians from Medellin, Colombia (CLM), Mexican Ancestry from Los Angeles USA (MXL), Peruvians from Lima, Peru (PEL), Puerto Ricans from Puerto Rico (PUR). EAS: Chinese Dai in Xishuangbanna, China (CDX), Han Chinese in Beijing, China (CHB), Southern Han Chinese (CHS), Japanese in Tokyo, Japan (JPT), Kinh in Ho Chi Minh City, Vietnam (KHV). EUR: Utah Residents (CEPH) with Northern and Western European Ancestry (CEU), Finnish in Finland (FIN), British in England and Scotland (GBR), Iberian Population in Spain (IBS), Toscani in Italia (TSI). SAS: Bengali from Bangladesh (BEB), Gujarati Indian from Houston, Texas (GIH), Indian Telugu from the UK (ITU), Punjabi from Lahore, Pakistan (PJL) and Sri Lankan Tamil from the UK (STU).

LDproxy tools of LDlink 4.0.3 web based suite (https://ldlink.nci.nih.gov/) was used to map proxy variants in strong LD and with putatively functional role. LDpop tool of the LDlink 4.0.3 was used for geographically

annotating allele frequencies in 1000G populations, alternatively also done by a web based tool Data wrapper (https://www.datawrapper.de/) in some of the figures.

Computational structural analysis on SARS-CoV-2 S-protein and TMPRSS2

TMPRSS2 has been recently characterized as critical component for cell entry by SARS-CoV-2 (Hoffmann, et al., 2020). To understand, the interactions, the protein sequence of surface glycoprotein (YP_009724390.1) of SARS CoV-2 and two transcripts of TMPRSS2 (NP_005647.3 and NP_001128571.1) protein of homo sapiens, were retrieved from the NCBI-Protein database. Pairwise sequence alignment of TMPRSS2 isoforms was carried out by Clustal Omega tool (Sievers, et al., 2011). The protein domain information and transcript variation were retrieved from Uniport (UniProt, 2019), Prosite (Sigrist, et al., 2013), Pfam (El-Gebali, et al., 2019) and ENSEMBL (Chen, et al., 2010), respectively. The homology model of the S-protein and TMRPSS2 constructed using Swiss model (Waterhouse, et al., 2018), whereas 3D structure of the ACE2 retrieved from the PDB database (PDB ID: 6M17). These structures were energy minimized by the Chiron energy minimization server (Ramachandran, et al., 2011). The binding site residues of the proteins retrieved from Uniport and literature. The mutant structure of the TMRPSS2 protein was generated using WHATIF server (Chinea, et al., 1995) and energy minimized. The effect of the mutant was analysed using HOPE (Venselaar, et al., 2010) and I-mutant (Capriotti, et al., 2006). The I-mutant method allows us to predict stability of the protein due to mutation. The docking studies for wild and mutant TMRPSS2 with S-protein and ACE2 carried out using HADDOCK (Dominguez, et al., 2003).

Network analysis on SARS-CoV-2 with Human Proteins

We downloaded the SARS-CoV-2 genome (Accession number: MT121215) from the NCBI database. In order to find the Host-Pathogen Interactions (HPIs), the SARS-CoV-2 protein sequences were subjected to Host-Pathogen Interaction Database (HPIDB 3.0) (Ammari, et al., 2016; Kumar and Nanduri, 2010). In addition to other host genes, we added two more genes (*TMPRSS2* and *SLC6A19*) which found to have an important role in the mechanism of viral entry (Hoffmann, et al., 2020). The protein-protein interaction (PPI) and transcription factor regulation of human proteins were retrieved from GeneMANIA (Warde-Farley, et al., 2010) and literature (Barros, et al., 2012; David, et al., 2010; Maitland, et al., 2011; Tumer, et al., 2013; Yu, et al., 2010; Zhang, et al., 2009), respectively. The Host Pathogen Interaction Network (HPIN) was visualized using Cytoscape (Shannon, et al., 2003) which includes the information collected from HPIDB, PPIs and TFs. Modules are defined as the set of statistics and functionally significant interacting genes (Reichardt and Bornholdt, 2006) which is constructed by using MCODE (Bader and Hogue, 2003). Further, Hubs were identified using Network analyzer (Assenov, et al., 2008), the plugin of Cytoscape v3.2.1. We also studied the hub proteins association with diseases using DisGeNET (Menche, et al., 2015).

The topological properties of the network and their functional significance can be studied within the formalism of network theory and can predict important organizational and regulatory candidates in the network. We used

network theoretical concepts, namely probability of degree distribution, clustering coefficient and average neighborhood connectivity, to characterize the structural and organizational features of the network (Details in supplementary Information). Removal of high degree nodes (hubs) in biological networks may cause lethality to the corresponding organism; the phenomenon has been referred to as the centrality–lethality rule (Jeong, et al., 2001), verified by various genomic investigations. This idea of understanding may enable us to determine the topological features of the network architecture, important functionally related modules and hubs (Malik, et al., 2019; Nafis, et al., 2016). The topological properties were calculated after each subsequent removal using the Network Analyzer plugin in Cytoscape version 3.7.1. The calculated topological properties of knock-out experiment were compared with those of the main network and the change in the properties helped in understanding the role of leading hubs in the network.

Results and Discussion

SARS-CoV-2 uses ACE2 for entry and its S-protein priming by the serine protease TMPRSS2 is key factor. Other proteases like cathepsin B and L may be available in host cells yet only TMPRSS2 activity is essential for pathogenesis and spread (Hoffmann, et al., 2020).

Dynamics and binding analysis of ACE2 with SARS CoV-2 RBD in dimeric and monomeric state

Mutagenesis experiments have reported the importance of Arginine and Lysine residues in ACE2 positioned between 697 to 716 as an important recognition site for TMPRSS2 mediated cleavage **(Figure S1A)** of ACE2. Mapping these residues on the recently resolved structure (61M7.pdb) suggests that this region lies in symmetric dimerization interface between ACE2 homodimer and is also masked from outside by two BoAT1 in an overall 1:2:1 hetero-tetramer of B0AT1 and ACE2 **(Figure S1A)** (Yan and Zhang, 2020)**.** In a recently reported study, the overexpression of *ACE2* has been reported to have an overall protective role in viral infection among patients (Imai, et al., 2005). Increased density of ACE2 on the cell surface has been observed to protect from lung injury (Imai, et al., 2005) also been observed at many other instances. We propose increased expression of ACE2 due to various factors, including natural occurring variations influencing expression of the gene, may increase collisions and hence result in homo-dimerization of this protein. Binding of B0AT1 to ACE2 is not dependent on ACE2 homodimerization, but its presence along with dimerised ACE2 effectively shields the later from interaction with TMPRSS2 and may prevent it or reduce its efficiency to cleave ACE2, a hypothesis based on visualization of the available experimentally resolved structure 61M7.PDB (Yan and Zhang, 2020). This observation is significant since the cleaved ACE2 interacts more efficiently with the SARS CoV-2 RBD domain.

Additionally, we also explored if the protease domains (PD) of each of the homodimerized ACE2 could independently bind with whole of the Spike Glycoprotein without effecting each other or any steric hindrance (Yan and Zhang, 2020). As there is lack of any experimentally resolved structure available in literature with

ACE2 homodimer and complete SARS-CoV2 Spike Glycoproteins binding to these, we aligned the RBD domains of the 6M17.pdb with the prefusion SARS-CoV2 Spike Glycoprotein in the optimal ACE2 binding conformation (Song, et al., 2018) with "up CTD1" and "open S1 subunit" (**Figure 1')**. Both Spike Glycoproteins (6VSB.pdb) aligned well with viral RBD of (6M17.pdb). Further these were also observed without any steric clash with the ACE2 or partner Spike Glycoprotein in modelled structure. Both of these protruded radially outward from ACE2 binding site but inwards, at anchorage sites on virus membrane, with distance of approximately 27 nanometers (nm) (**Figure 1')**. However, considering the reported inter spike distance, between 13-15 nm (Neuman, et al., 2006) and relative positions of Spike proteins on the viral shell, given almost similar sizes of SARS-CoV (Goldsmith, et al., 2004; Neuman, et al., 2006) and SARS-CoV-2 (Chen, et al., 2020), these are anticipated to be either parallel or protruding radially outwards from its anchorage site, contrasting to the findings in modelled structure (**Figure 1')**. With this finding of inverse orientation of the Spike protein from virus shell in modelled structure, we propose that in case of ACE2 dimerization, only one of the dimerized ACE2 can bind with the Spike protein due to steric hinderances. Thus, the other unbound ACE2 partner may participate in its physiological role and continue to protect from lung injury.

To understand the mechanistic effect of dimerization, we conceived and simulated two situations: one, where ACE2 dimer is bound to two B0AT1 and two, RBD domains of SARS CoV-2 and second, where only monomeric ACE2 is bound to one viral RBD. From the RMSF analysis of the simulated trajectories, we observed higher order fluctuation in monomeric ACE2 homo-dimerization interface while the rest of the ACE2 displayed a similar fluctuation profile including residues interacting with RBD **(Figure S1'')**. PCA analysis and amino acid residue loadings on the PCs (PC1 in this case) reported slightly higher away ward conformational dynamics w.r.t RBD in dimeric ACE2 **(Figure S1'')**. This contrasting essential dynamics in dimeric ACE2 is explained well through the MM-GBSA based free energy of binding calculation between the 10th nanosecond final confirmation of ACE2-RBD complex. From both simulations through MM-GBSA method, 1.5 fold strong binding of monomeric ACE2-RBD complex compared to dimeric ACE2-RBD was observed (*i.e.* ΔG=-75.58 for Dimeric ACE2-RBD vs ΔG=-116.98 for Monomeric ACE2-RBD Complex). This observation further explains the protective role of overexpressed ACE2, resulting in its dimerization and reduced affinity for the RBD domain of SARS CoV-2 S1 protein. However, we are also not clear whether the presence of B0AT1 has any allosteric effect on this observation, in addition to already observed masking of ACE2 from TMPRSS2 mediated cleavage. Additionally, another metalloprotease ADAM17 has been reported to compete with the TMPRSS2 and cleaves ACE2 in a way that only cleavage by TMPRSS2 was reported to drive the SARS CoV entry inside the cell (Heurich, et al., 2014), which is yet to be explored in relation to SARS CoV-2. Recent literature also indicated the potential role of other proteases like cathepsin B/L that can functionally replace TMPRSS2, need to be evaluated extensively. (Sungnak, et al., 2020) All these hypotheses

warrant further *in-silico* analyses with better computational resources, as well as experimental study designs and for these we are open to seek collaborations.

Yet, the observations made are of high importance and emphasise on evaluation of expression of the ACE2 and BoAT1 along with TMPRSS2 among patients with varied clinical response to SARS CoV-2 infection, differential outcomes and correlation with observed mortality. Therefore differential expression of these genes among patients with displaying varied responses from asymptomatic to acute symptoms is worth an exploration which may act as biomarkers if proven, to predict severity and susceptibility.

Differential Genomics backgrounds derived expression of *ACE2* and *TMPRSS2*

The observations, from our MD analyses **(Figures S1'')** show that higher expression of ACE2 gene may promote ACE2 homo-dimerization rendering less binding affinity to SARS CoV-2 RBD as well as masking TMPRSS2 cleavage site **(Figure 1).** Eevidences on eQTLs and ACE2 higher expression in East Asians (Chen, et al., 2020) and reported protective role of ACE2 in lung injury (Imai, et al., 2005). We explored more about ACE2 expression as well as differential genomic backgrounds in different population groups.

***ACE2* Expression and functional SNPs related to its expression**

Tissue Specific evaluation of ACE2 gene in GTEx portal indicated low level expression of the ACE2 in Lungs (**Figure S2a and Figure S3**). Further, it was observed that not all the transcripts and exons of the gene express in Lungs (**Figure S2b and c**). As expression of *ACE2* is less in Lungs thus, probably GTEx portal did not return cis-eQTLs for *ACE2* gene in lungs. However, eQTLs for the gene were found in other tissues **(Figure 2a and b)** in GTEx portal. These eQTLs remained the same across tissue sets and showed similar effect patterns in expression (**Figure 2b)**. Yet to corelate the expression of the gene with genomic variations, regions of the gene were explored for potential regulatory elements and overlapped it with common variations through table browser tool of UCSC genome browser with assumption that the variants having population level effect should be common variants **(Figure S2d and S4).** Variations data was retrieved from 1000 Genomes Phase 3 dataset and filtered for variants with at least 10% frequency of the alternate allele in global population. Overlapping the variants from both the exercises resulted in shortlisting of 2 SNPs rs1978124 and rs2106809, which were observed with differential frequency distribution in different populations of the world **(Figure S5)** at both super population group and sub population group level. Interestingly, EAS and EUR sub population groups were observed to show relatively uniform frequency distribution within group. However, in AFR, AMR and SAS sub population groups intra population group differences were observed to be higher, indicating diversity in the gene pool of population groups. HaploReg annotations indicated that these SNPs are in region with Enhancer histone marks and DNAase activity as well as the same were observed through multiple regulatory elements tracks in UCSC Genome browser **(Figure S2d and S4)** including GH0XJ015596

enhancer marked by GeneHancer database. (Fishilevich, et al., 2017) Linkage Disequilibrium (LD) values as (r^2) with other putative proxy functional variants was also explored and mapped with UCSC genome browser. Interestingly, it was observed that SNPs rs1978124 and rs2106809 have a strong LD block of >100kb with various SNPs in absolute LD but upstream of ACE2 gene across population groups **(Figure S6)**. This indicates a strong enhancer activity from the region that may affect higher expression of ACE2 gene in lungs, which may facilitate ACE2 homo-dimerization (**Figure 1**). However, it also requires experimental validation.

***TMPRSS2* Expression and functional SNPs in the gene with potential effect**

GTEx portal indicated relatively high levels of *TMPRSS2* expression in Lungs (**Figure S2a and S7c**), differential transcription (**Figure S7c**) but no protein expression in lungs (**Figure S7a**). Evaluation of the Protein atlas portal, source of Figure ~~10a~~ S7a, indicated that both antibodies used for detection TMPRSS2 (not shown in Ms) were restricted to target near N terminal of the protein (either cytoplasmic domain or proximal extracellular domain near membrane). Evaluation of the GTEx portal for cis-eQTLs for TMPRSS2 gene in lungs, returned a large number of eQTLs but with a peculiar feature (**Figure 3a and b**). The eQTLs in lungs were different as compared to other tissues and found to be concentrated in region of the gene with potential alternate transcripts (**Figure 4a,b and S8**), towards end of the gene in relatively high expressing exons (**Figure 4b)** and coding for the amino acid sequence that has putative functional role in protein as serine protease domain **(Figure 4a)** critical for ACE2 cleavage and SARS CoV-2 S-Protein priming. Variations data was retrieved from 1000 Genomes Phase 3 dataset and filtered for variants with at least 10% frequency of the alternate allele in global population and overlapped it with cis-eQTLs data resulting in 10 SNPs (rs463727, rs55964536, rs4818239, rs734056, rs4290734, rs2276205, rs34783969, rs11702475, rs62217531 and rs383510). Annotation of the SNPs indicated all the SNPs cluster together and are in strong LD block **(Figure S8 and S9a)**. HaploReg annotations indicated Enhancer histone marks and DNAase activity in the regions overlapping these SNPs amongst these rs4818239 showed a prominent putative functional role (**Figure S9b**) which further requires experimental validation. However, the frequency distribution of the variant rs4818239 in different populations groups of 1000G showed interesting differential pattern (**Figure S9c**). We also explored if there are any alternate functional variations, yet common in populations exist by screening TMPRSS2 gene through genomAD browser and filtered for missense only variations. The search returned rs75603675 (NP_001128571.1:p.Gly8Val or G8V) and rs12329760 (NP_001128571.1:p.Val197Met or V197M), also observed with differential frequency distribution in 1000G populations (**Figure S9d and e**). The observations indicate *TMPRSS2* variants may influence interaction with *ACE2* as well as SARS CoV-2 (**Figure 1**) resulting in population specific differential outcomes.

The variation in TMPRSS2 could inhibit the ingress of SARS-CoV-2

We further opted to explore more the structure and function of TMPRSS2 protein. Pairwise sequence alignment of two isoforms of TMPRSS2 suggests that Isoform-2 lack 37 residues at N-terminal compare to Isoform-1, which was the longest transcript and codes for 529 amino acids (**Figure S10**). Since the human TMPRSS2 protein structure was not available in the PDB database, we have generated the computational protein model. The model built using Serine protease hepsin (PDB ID: 5CE1) of homo sapiens. The protein 3D structure modelled from 146-491 residues of TMPRSS2 with sequence identity, GMQE and QMEAN of 33.82%, 0.53 and -1.43 values, respectively. It showed that the model was constructed with high confidence and best quality. In the similar manner 3D structure of S-Protein of SARS-CoV-2 was built with sequence identity, GMQE and QMEAN of 99.26%, 0.72 and -2.81 values, respectively. The protein stability analysis showed that rs12329760 (p.Val197Met or V197M) (Isoform-1) variation could decrease the stability of TMPRSS2 protein with ΔΔG value of -1.51 kcal/mol. The HOPE results suggest, V197M variation is located within a domain, SRCR (GO Term: Scavenger Receptor Activity as annotated in UniProt) and introduces an amino acid with different properties, which could disturb this domain and can abolish its function. Analyses of another variation rs75603675 (p.Gly8Val or G8V) showed that wild-type residue, glycine flexibility might be necessary for the protein function and alteration in this position can abolish this function as the observed torsion angles for this residue were unusual. It could be speculated that only glycine was flexible enough to make these torsion angles, change at the location into another residue would force the local backbone into an incorrect conformation and may disturb the local structure. The variant residue was also observed to be more hydrophobic than the wild-type residue. Since sequence similarity search did not find any significant template at the N-terminal of this protein, we could not generate a quality model for isoform-2, which contains G8V variation; hence we carried out sequence-based stability analysis. The results suggest G8V variation could increase the stability of the TMPRSS2 protein with ΔΔG value of -0.10 kcal/mol. Further, it is known that Arginine and lysine residues within amino acids 697 to 716 are essential for efficient ACE2 cleavage by TMPRSS2 (Heurich, et al., 2014) and recent studies have shown that SARS-CoV-2 uses the ACE2 for entry and the serine protease TMPRSS2 for S-protein priming. Based on information from previous studies, we docked the TMPRSS2 p.Val197Met wild-type and variant protein with ACE2 and S-protein of SARS-CoV-2. The docking results suggest that the variant 197M protein could promote the binding to ACE2 and inhibit the binding with S-protein (**Figure S11**). However, these observations need critical revaluation as well as experimental work to understand these interactions better.

***SLC6A19* (B0AT1) if expresses naturally in Lungs and other respiratory tract cells, may provide protection.**

One of the interesting gene is *SLC6A19* that codes for protein B0AT1 that expresses in very limited number of tissues and reported absent in Lungs (**Figure S2a -and S12a,b,c**). Our findings indicated its protective role with competitive hinderance in binding to TMPRSS2. As its expression was observed to be very low in Lungs

we resolved to look for indirect signatures that may have putative role in providing differential susceptibility. We noticed several variations clustering together in a potential enhancer region (**Figure S12d and e**) and with differential frequencies in different populations. eQTL analyses at GTEx portal also showed huge list of potential SNPs upregulating or down regulating *SLC6A19* expression in Pancreas, liver and whole blood cells as well as with overlap with potential Transcription factor binding sites (**Figure S12f)**. We hypothesize a potential chance of some natural occurring variation/s that can induce expression of BoAT1 in respiratory tract thus providing protective role in this scenario (**Figure 1**). However, this requires more extensive computational exploration as well as experiential validations.

Host-Pathogen Interaction Modelling

We believed additional genes and factors might be playing role thus, we further carried out a systems biology study to identify these novel key regulators that may influence this Human and SARS CoV-2 interaction. A detailed Host Pathogen Interaction Network (HPIN) was created. The constructed HPIN contained 163 interactions, involving 31 nodes, which includes 4 viral proteins, 27 human proteins and 8 Transcription Factors (TF) (**Figure 5A**). From the HPIN, we identified hubs, namely *RPS6*, *NACA*, *HNRNPA1*, *BTF3* and *SUMO1* with 19, 18, 17, 16 & 12 degrees, respectively in the network (**Figure 5A**). This indicates the affinity to attract a large number of low degree nodes towards each hub, which is a strong evidence of controlling the topological properties of the network by these few hubs (Good, et al., 2011). Interestingly, out of five significant hubs, four hubs (*RPS6*, *NACA*, *HNRNPA1* and *BTF3*) present in module (Nodes: 16, Edges: 118, Score: 15.73) and one hub *SUMO1* is present at motif level which considered one of the most important regulating motif of biological network at a fundamental level (**Figure 5B**). From our prediction; we found, four viral proteins (*S*, *N*, *ORF1a* & *ORF1ab*) target five host protein groups (*ACE2*, *SUMO1*, *HNRNPA1*, *RPS6* & *ATP6V1G1*). *SUMO1* & *HNRNPA1* are target by same viral proteins (N). The hub protein, *RPS6* (highest degree) directly interacts with one of the important protein *TMPRSS2* which further propagate the signal to *ACE2 & SLC6A19*. The Transcription factor HIF1A and BCL6, STAT5, YBX1 inhibits *ACE2* and *SUMO1* whereas MYC, AR and HNF4a, HNF1a activates *HNRNPA1*, *TMPRSS2* and *SLC6A19* respectively. From the gene diseases association study few diseases are highly associated with these important hub proteins (**Figure S13A**); *HNRNPA1* (36%) followed by *RPS6* (25%), *SUMO1* (21%), *BTF3* (9%) and *NACA* (9%) (**Figure S13B**). Clinically, patients with COVID-19 present with respiratory symptoms, Anoxia, fatigue, heart failure etc. are associated with these five hub proteins mainly *HNRNPA1& SUMO1*.

By hub removal methodology; we tried to understand the effect of hub removal and calculated the topological properties of the HPIN as a control. The probability of degree distribution P(k) showed that the HPIN followed a power law scaling behavior. The power law behavior was also checked and confirmed by using statistical test for power law fitting (p-value≥0.1)(Clauset, et al., 2009) in the hub-removal process. The hub removal analysis showed an important magnitude of changes in network metrics such as Degree distribution (Indegree & outdegree), Clustering coefficient and Neighborhood connectivity (**Figure S14A**). This shows that

removing *RPS6*, *HNRNPA1*, *SUMO1*, *NACA* & *BTF3* leading hubs from the network allows more responsibilities of the existing leading hubs in the resulting network in order to reorganize and save the network properties from breakdown. The Indegree and Outdegree distribution of HPIN showed the removal of *NACA, RPS6* & *SUMO1* differ from the complete (**Figure S14B**). In case of clustering coefficient, the increase in γ indicates the increase in compactness in the hubs removed network in order to save the network from breakdown. Perturbation of *BFT3* shows minimum γ, indicating removal of *BFT3* makes the network less compact, which may lead to the delay in flow of signal. In Neighbourhood connectivity with exponent μ which is maximum in removal of *SUMO1* hub, which reveals that the regulating roles of remaining hubs become more important (Borgatti, et al., 2006). The increase in μ indicates that the information processing in the network becomes faster when *SUMO1* hubs are removed which means that local perturbations due to removal of hubs are strong enough to cause significant change in global scenario (Canright and Engø-Monsen, 2004) (**Figure S14B**). This indicated the assortivity nature i.e hubs are important but if we remove the hub there will be no break-down of the network. Therefore, the knock out hub experiments in HPIN shows no drastic change in the topological properties of the perturbed network, but enhance the regulating capabilities of the modules than the hubs, which is the consequence of strong inter-links in the network.
Overall network analysis showed *ACE2* is not only the key molecule for entry and survival of SARS-CoV-2 virus, the hub proteins like *RPS6*, *HNRNPA1*, *SUMO1*, *NACA* & *BTF3* might also play a vital role. Analysing these interactions could provide further important understanding for the underlying biological mechanism of SARS-CoV-2 virus infection and identifying putative drug targets.

To conclude (**Figure 1**), higher expression of *ACE2* is facilitated by natural variations with different frequencies in different populations and is functionally associated with expression of the gene. The higher expression of ACE2 facilitates homo-dimerization resulting in hindrance to TMPRSS2 mediated cleavage of ACE2. It becomes more difficult in presence of B0AT1 that usually does not express in Lungs. We also propose that the monomeric ACE2 has higher preferential binding with SARS-CoV-2 S-Protein vis-a-vis its dimerized counterpart. Further, natural variations in *TMPRSS2*, with potential functional role, and their differential frequencies may also result in differential outcomes towards interaction with ACE2 or priming of viral S-protein, a critical step for entry of virus in host cells. In addition, we have identified some other potential key host genes like *ADAM17, RPS6, HNRNPA1, SUMO1, NACA* and *BTF3,* that might have a critical role. With all this background, it is anticipated that in populations like Indian populations, with highly diverse gene pool, a great variation in clinical outcomes is expected and that could be population/region specific, but primarily due to gene pool structure of the region, despite similar exposure levels to SARS CoV-2 and resources. Understanding these population specific differences may help in developing appropriate management strategies.

Acknowledgment
All the authors acknowledge Prof. RNK Bamezai (Padamshri), former Vice Chancellor Shri Mata Vaishno Devi University, Katra and former Professor and Coordinator, National Centre for Applied Human Genetics, School of Life Sciences, Jawaharlal Nehru University, New Delhi, for his critical suggestions through various virtual discussion rounds, resulting in present study design. Authors also acknowledge Prof. Gyaneshwar Chaubey, Banaras Hindu University, UP, India for inputs, suggestions and assistance with geographical mapping of the allele frequencies from 1000G dataset.

Author Contributions
SS conceived the concept. IP carried out molecular modelling simulations of ACE2 and related analyses. KP carried out TMPRSS2 modelling and related analyses. SS and ER carried out Human Population data screening and related work. SH and MZM carried out network analyses to identify additional key genes. SS, IP, SH, MZM designed, analysed, executed and wrote their part of manuscript. SS interpreted the results together, ER assisted SS in compilation of figures and SS compiled the overall MS.

Competing Interests
The authors declare no competing interests associated with MS. For declaration purposes, SS is founder, chief scientific advisor of a startup “Biodroid Innovations Pvt Ltd” and IP is director of “Bioinfores Pvt. Ltd.”.

REFERENCES

Proceedings of the 2006 ACM/IEEE conference on Supercomputing. In. Tampa, Florida: Association for Computing Machinery; 2006.

Ammari, M.G., *et al.* HPIDB 2.0: a curated database for host-pathogen interactions. *Database (Oxford)* 2016;2016.

Assenov, Y., *et al.* Computing topological parameters of biological networks. *Bioinformatics* 2008;24(2):282-284.

Bader, G.D. and Hogue, C.W. An automated method for finding molecular complexes in large protein interaction networks. *BMC Bioinformatics* 2003;4:2.

Barros, P., *et al.* Rac1 signalling modulates a STAT5/BCL-6 transcriptional switch on cell-cycle-associated target gene promoters. *Nucleic Acids Res* 2012;40(16):7776-7787.

Borgatti, S., Carley, K. and Krackhardt, D. On the Robustness of Centrality Measures Under Conditions of Imperfect Data. *Social Networks* 2006;28:124-136.

Canright, G. and Engø-Monsen, K. Roles in networks. *Science of Computer Programming* 2004;53(2):195-214.

Cao, Y., *et al.* Comparative genetic analysis of the novel coronavirus (2019-nCoV/SARS-CoV-2) receptor ACE2 in different populations. *Cell Discov* 2020;6:11.

Capriotti, E., Calabrese, R. and Casadio, R. Predicting the insurgence of human genetic diseases associated to single point protein mutations with support vector machines and evolutionary information. *Bioinformatics* 2006;22(22):2729-2734.

Chen, J., *et al.* Individual Variation of the SARS-CoV2 Receptor ACE2 Gene Expression and Regulation. *Pre prints* 2020:preprints.org > 202003.200191.v202001.

Chen, N., *et al.* Epidemiological and clinical characteristics of 99 cases of 2019 novel coronavirus pneumonia in Wuhan, China: a descriptive study. *Lancet* 2020;395(10223):507-513.

Chen, Y., *et al.* Ensembl variation resources. *BMC Genomics* 2010;11:293.

Chinea, G., *et al.* The use of position-specific rotamers in model building by homology. *Proteins* 1995;23(3):415-421.

Clauset, A., Shalizi, C.R. and Newman, M.E.J. Power-Law Distributions in Empirical Data. *SIAM Review* 2009;51(4):661-703.

David, C.J., *et al.* HnRNP proteins controlled by c-Myc deregulate pyruvate kinase mRNA splicing in cancer. *Nature* 2010;463(7279):364-368.

Dominguez, C., Boelens, R. and Bonvin, A.M. HADDOCK: a protein-protein docking approach based on biochemical or biophysical information. *J Am Chem Soc* 2003;125(7):1731-1737.

El-Gebali, S., *et al.* The Pfam protein families database in 2019. *Nucleic Acids Res* 2019;47(D1):D427-D432.

Fishilevich, S., *et al.* GeneHancer: genome-wide integration of enhancers and target genes in GeneCards. *Database (Oxford)* 2017;2017.

Goldsmith, C.S., *et al.* Ultrastructural characterization of SARS coronavirus. *Emerg Infect Dis* 2004;10(2):320-326.

Good, M.C., Zalatan, J.G. and Lim, W.A. Scaffold proteins: hubs for controlling the flow of cellular information. *Science* 2011;332(6030):680-686.

Grant, B.J., *et al.* Bio3d: an R package for the comparative analysis of protein structures. *Bioinformatics (Oxford, England)* 2006;22(21):2695-2696.

Guan, W.J., *et al.* Clinical Characteristics of Coronavirus Disease 2019 in China. *N Engl J Med* 2020.

Heurich, A., *et al.* TMPRSS2 and ADAM17 cleave ACE2 differentially and only proteolysis by TMPRSS2 augments entry driven by the severe acute respiratory syndrome coronavirus spike protein. *J Virol* 2014;88(2):1293-1307.

Hoffmann, M., *et al.* SARS-CoV-2 Cell Entry Depends on ACE2 and TMPRSS2 and Is Blocked by a Clinically Proven Protease Inhibitor. *Cell* 2020.

Humphrey, W., Dalke, A. and Schulten, K. VMD: Visual molecular dynamics. *Journal of molecular graphics* 1996;14(1):33-38.

Imai, Y., *et al.* Angiotensin-converting enzyme 2 protects from severe acute lung failure. *Nature* 2005;436(7047):112-116.

Jacobson, M.P., *et al.* On the Role of the Crystal Environment in Determining Protein Side-chain Conformations. *Journal of molecular biology* 2002;320(3):597-608.
Jeong, H., *et al.* Lethality and centrality in protein networks. *Nature* 2001;411(6833):41-42.
Kaiser, J. How sick will the coronavirus make you? The answer may be in your genes. *Health, Coronavirus, Sciencemag.org* 2020.
Kumar, R. and Nanduri, B. HPIDB--a unified resource for host-pathogen interactions. *BMC Bioinformatics* 2010;11 Suppl 6:S16.
Kuster, G.M., *et al.* SARS-CoV2: should inhibitors of the renin-angiotensin system be withdrawn in patients with COVID-19? *Eur Heart J* 2020.
Madhavi Sastry, G., *et al.* Protein and ligand preparation: parameters, protocols, and influence on virtual screening enrichments. *Journal of computer-aided molecular design* 2013;27(3):221-234.
Maitland, N.J., *et al.* Prostate cancer stem cells: do they have a basal or luminal phenotype? *Horm Cancer* 2011;2(1):47-61.
Malik, M.Z., *et al.* Methodology of predicting novel key regulators in ovarian cancer network: a network theoretical approach. *BMC Cancer* 2019;19(1):1129.
Mark, P. and Nilsson, L. Structure and Dynamics of the TIP3P, SPC, and SPC/E Water Models at 298 K. *The Journal of Physical Chemistry A* 2001;105(43):9954-9960.
Menche, J., *et al.* Disease networks. Uncovering disease-disease relationships through the incomplete interactome. *Science* 2015;347(6224):1257601.
Miller, A., *et al.* Correlation between universal BCG vaccination policy and reduced morbidity and mortality for COVID-19: an epidemiological study. *medRxiv* 2020:2020.2003.2024.20042937.
Monteil, V., *et al.* Inhibition of SARS-CoV-2 Infections in Engineered Human Tissues Using Clinical-Grade Soluble Human ACE2. *Cell* 2020.
Nafis, S., *et al.* Identification of key regulators and their controlling mechanism in a combinatorial apoptosis network: a systems biology approach. *Mol Biosyst* 2016;12(11):3357-3369.
Neuman, B.W., *et al.* Supramolecular architecture of severe acute respiratory syndrome coronavirus revealed by electron cryomicroscopy. *Journal of virology* 2006;80(16):7918-7928.
Ramachandran, S., *et al.* Automated minimization of steric clashes in protein structures. *Proteins* 2011;79(1):261-270.
Reichardt, J. and Bornholdt, S. Statistical mechanics of community detection. *Physical Review E* 2006;74(1):016110.
Shannon, P., *et al.* Cytoscape: a software environment for integrated models of biomolecular interaction networks. *Genome Res* 2003;13(11):2498-2504.
Shi, Y., *et al.* COVID-19 infection: the perspectives on immune responses. *Cell Death Differ* 2020.
Sievers, F., *et al.* Fast, scalable generation of high-quality protein multiple sequence alignments using Clustal Omega. *Mol Syst Biol* 2011;7:539.
Sigrist, C.J., *et al.* New and continuing developments at PROSITE. *Nucleic Acids Res* 2013;41(Database issue):D344-347.
Song, W., *et al.* Cryo-EM structure of the SARS coronavirus spike glycoprotein in complex with its host cell receptor ACE2. *PLoS Pathog* 2018;14(8):e1007236.
Stawiski, E.W., *et al.* Human ACE2 receptor polymorphisms predict SARS-CoV-2 susceptibility. *bioRxiv* 2020:2020.2004.2007.024752.
Sungnak, W., *et al.* SARS-CoV-2 entry factors are highly expressed in nasal epithelial cells together with innate immune genes. *Nature Medicine* 2020.
Tumer, E., *et al.* Enterocyte-specific regulation of the apical nutrient transporter SLC6A19 (B(0)AT1) by transcriptional and epigenetic networks. *J Biol Chem* 2013;288(47):33813-33823.
Uhlen, M., *et al.* Proteomics. Tissue-based map of the human proteome. *Science* 2015;347(6220):1260419.
UniProt, C. UniProt: a worldwide hub of protein knowledge. *Nucleic Acids Res* 2019;47(D1):D506-D515.
Venselaar, H., *et al.* Protein structure analysis of mutations causing inheritable diseases. An e-Science approach with life scientist friendly interfaces. *BMC Bioinformatics* 2010;11:548.
Walls, A.C., *et al.* Structure, Function, and Antigenicity of the SARS-CoV-2 Spike Glycoprotein. *Cell* 2020.
Wan, Y., *et al.* Receptor Recognition by the Novel Coronavirus from Wuhan: an Analysis Based on Decade-Long Structural Studies of SARS Coronavirus. *Journal of Virology* 2020;94(7):e00127-00120.

Warde-Farley, D., *et al.* The GeneMANIA prediction server: biological network integration for gene prioritization and predicting gene function. *Nucleic Acids Res* 2010;38(Web Server issue):W214-220.
Waterhouse, A., *et al.* SWISS-MODEL: homology modelling of protein structures and complexes. *Nucleic Acids Res* 2018;46(W1):W296-W303.
Wrapp, D., *et al.* Cryo-EM structure of the 2019-nCoV spike in the prefusion conformation. *Science (New York, N.Y.)* 2020;367(6483):1260-1263.
Yan, R. and Zhang, Y. Structural basis for the recognition of SARS-CoV-2 by full-length human ACE2. 2020;367(6485):1444-1448.
Yu, Y.N., *et al.* Y-box binding protein 1 is up-regulated in proliferative breast cancer and its inhibition deregulates the cell cycle. *Int J Oncol* 2010;37(2):483-492.
Zhang, R., *et al.* Role of HIF-1alpha in the regulation ACE and ACE2 expression in hypoxic human pulmonary artery smooth muscle cells. *Am J Physiol Lung Cell Mol Physiol* 2009;297(4):L631-640.
Zhou, P., *et al.* A pneumonia outbreak associated with a new coronavirus of probable bat origin. *Nature* 2020;579(7798):270-273.

FIGURE LEGENDS

Figure 1. The overall interaction of host proteins and SARS-CoV-2 entry to cell

The figure summarises various factors involved that can influence the entry of Virus in host cell. It depicts brief mechanisms that may arise due to natural occurring variations influencing expression of host genes or structural changes affecting interactions within host proteins or viral proteins resulting in effect on efficiency of virus entry in host cells which could be key factor is providing differential clinical outcomes in different population groups. The figure depicts, higher expression of ACE2 is facilitated by natural variations with different frequencies in different populations and functionally associated with expression of the gene. The higher expression of ACE2 facilitates homo-dimerization resulting in hindrance to TMPRSS2 mediated cleavage of ACE2. Monomeric ACE2 has higher preferential binding with SARS-CoV-2 S-Protein vis-a-vis its dimerized counterpart. It becomes more difficult in presence of B0AT1 that usually does not express in Lungs. Further, natural variations in TMPRSS2, with potential functional role, and their differential frequencies may also result in differential outcomes towards interaction with ACE2 or priming of viral S-protein, a critical step for entry of Virus in host cells. In addition, other potential key host genes like ADAM17, RPS6, HNRNPA1, SUMO1, NACA and BTF3 might have a critical role.

Figure 1'. Complex of homo dimer of ACE2 with complete SARS-CoV-2 Spike Glycoprotein

Modelled complex of homo dimer of ACE2 colored as brick red (6M17.pdb) with complete Spike Glycoprotein in open state coloured as sky blue (6VSB.pdb) by aligning the complete Spike Glycoprotein with RBD colored as purple blue from 6M17.pdb. The head of the Spike protein can bind the dimer ACE2, protruding radially outward with RBD domains 6nm apart but inwards, at anchorage sites on virus membrane, with distance of approximately 27 nm.

Figure 2. The screenshot from GTEx portal depicting eQTLs of ACE2 Gene

eQTLs in different tissues were plotted through (a) GTEx IGV Browser as well as (b) GTEx Locus Browser. (a) Red dots indicate eQTLs that showed up in the region against the query. Size of the dot in (b) indicate level

of significance (as negative p values) whereas colour depicts positive or negative correlation with Normalized effect size (NES) of the eQTL from -1 to 0 to 1. Red color shades represent upregulation whereas blue color shades show downregulation. (b) also depicts Linkage disequilibrium (LD) with value range from 0 to 1 as white to black shades with 1(dark) as absolute LD.

Figure 3. The screenshot from GTEx portal depicting eQTLs of TMPRSS2 gene

eQTLs in different tissues were plotted through (a) GTEx IGV Browser as well as (b) GTEx Locus Browser. (a) Red dots indicate eQTLs that showed up in the region against the query. Size of the dot in (b) indicate level of significance (as negative p values) whereas colour depicts positive or negative correlation with Normalized effect size (NES) of the eQTL from -1 to 0 to 1. Red color shades represent upregulation whereas blue color shades show downregulation. (b) also depicts Linkage disequilibrium (LD) with value range from 0 to 1 as white to black shades with 1(dark) as absolute LD.

It was noted [also indicated by blue arrow in (a)] that where in other tissues eQTLs are mainly towards 5' UTR of the gene, in Lungs the eQTLs are towards end of the gene extending towards 3'UTR.

Figure 4. Structure of TMPRSS2 gene, its alternative transcripts and functional domains

(A) TMPRSS2 canonical transcript is constituted of 14 exons and alternate transcripts have been seen. The coded protein is a transmembrane protein with 1-85 amino acids (aa) forming Cytoplasmic Domain, and 112-492 aa constituting Extracellular domain. (B) Expression levels as median read count per base as shades of blue from low to high values indicating exons expression in different tissues in GTEx portal. Gene models of alternate transcripts are also depicted. Interesting to note exons coding for the extracellular domain have higher expression in Lungs (row marked by blue arrow) then other exons.

Figure 5. Host-Pathogen Interaction Network and their significant hubs.

(A) The network view of HPIN imported from Cytoscape. The Viral proteins, Human proteins and TFs are represented as nodes and edges denote the physical interaction. All the nodes of viral proteins (red), human proteins (blue) and TF (green) are filled triangles, circles and V-shaped respectively. The edges between Virus-human proteins are shown in orange-headed arrows, PPIs in grey lines and TF-human protein in pink arrow-headed (activators) and flat-headed (Inhibitors). The significant existence of sparsely distributed few main hub proteins, namely RPS6, NACA, HNPRNPA1, BTF3 and SUMO1 are colored as dark blue in the network were represented in the order of four enlarged sized circles.

(B) The Module and Motif constructed and analyzed using MCODE. All the nodes and edges of module & motif are in blue and grey color, respectively. The significant hubs, present in module & motif highlighted in dark blue color.

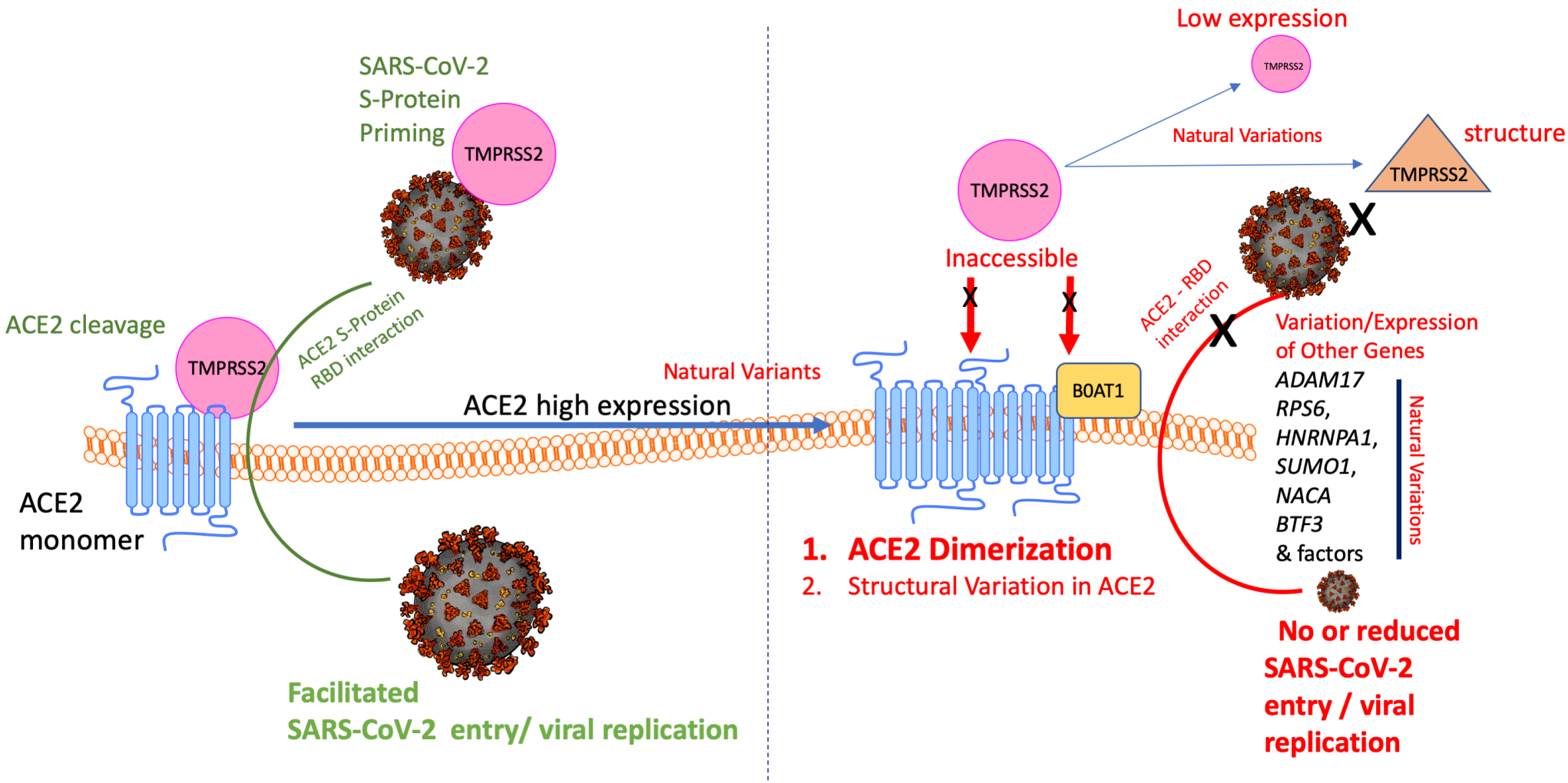
SARS-CoV-2
S-Protein
Priming
TMPRSS2
ACE2 cleavage
TMPRSS2
ACE2 S-Protein
RBD interaction
ACE2 high expression
ACE2
monomer
Facilitated
SARS-CoV-2 entry/ viral replication
Natural Variants
Low expression
TMPRSS2
Natural Variations
structure
TMPRSS2
TMPRSS2
Inaccessible
X
X
ACE2 - RBD
interaction
X
X
B0AT1
Variation/Expression
of Other Genes
ADAM17
RPS6,
HNRNPA1,
SUMO1,
NACA
BTF3
& factors
Natural Variations
1. ACE2 Dimerization
2. Structural Variation in ACE2
No or reduced
SARS-CoV-2
entry / viral
replication

Figure 1

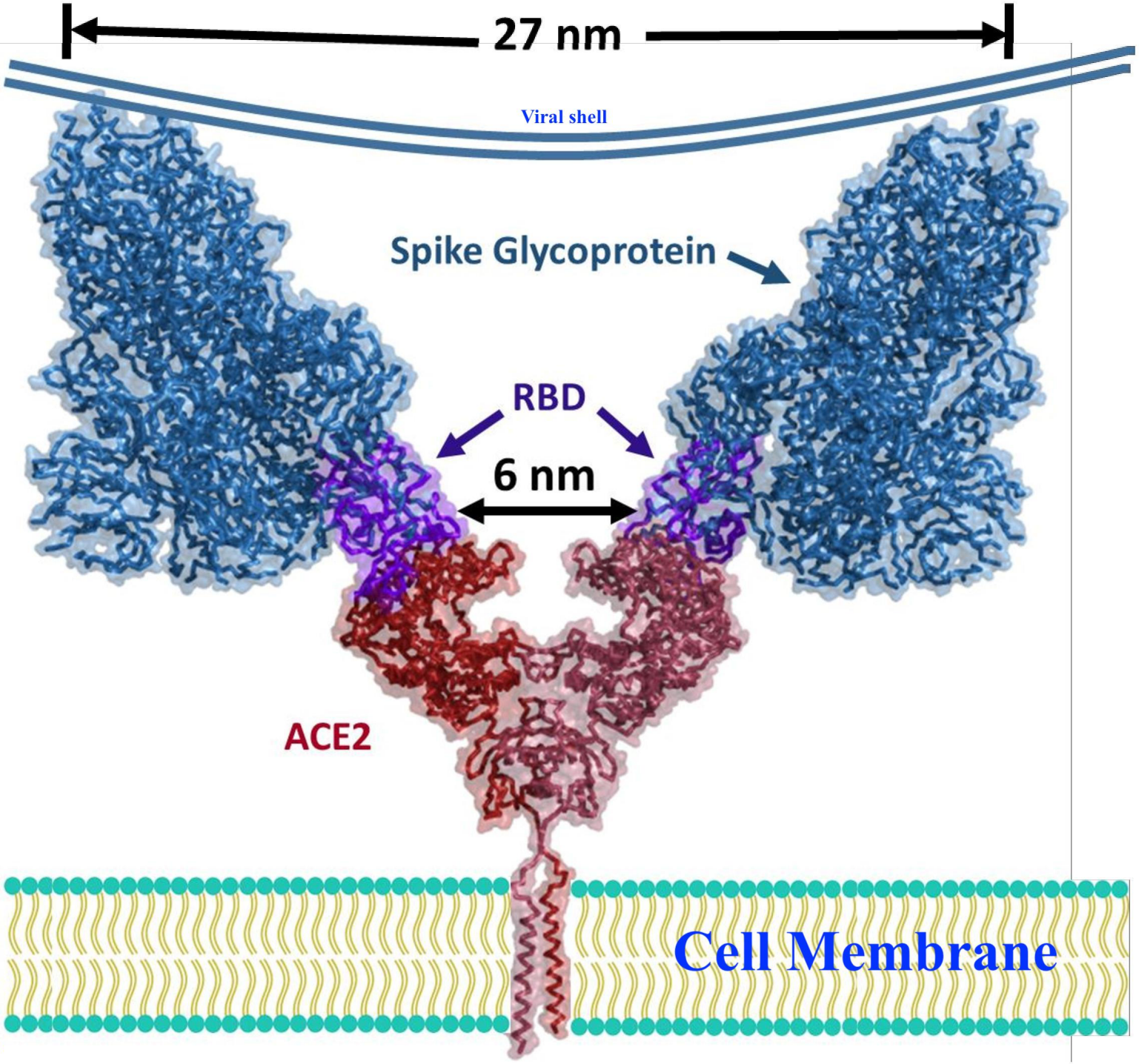
27 nm
Viral shell
Spike Glycoprotein
RBD
6 nm
ACE2
Cell Membrane

Figure 1'

a *ACE2* eQTLs various tissues

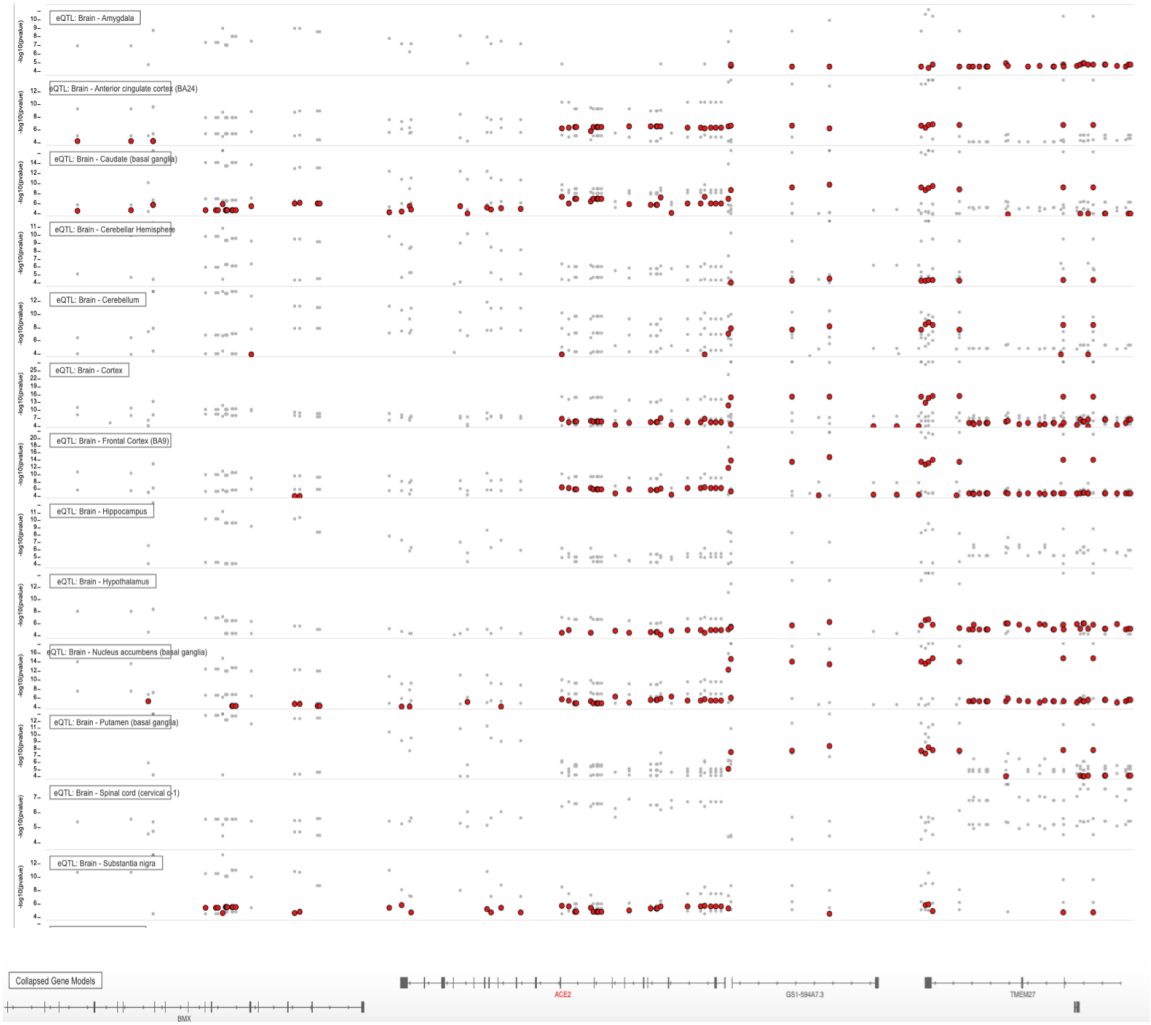

b

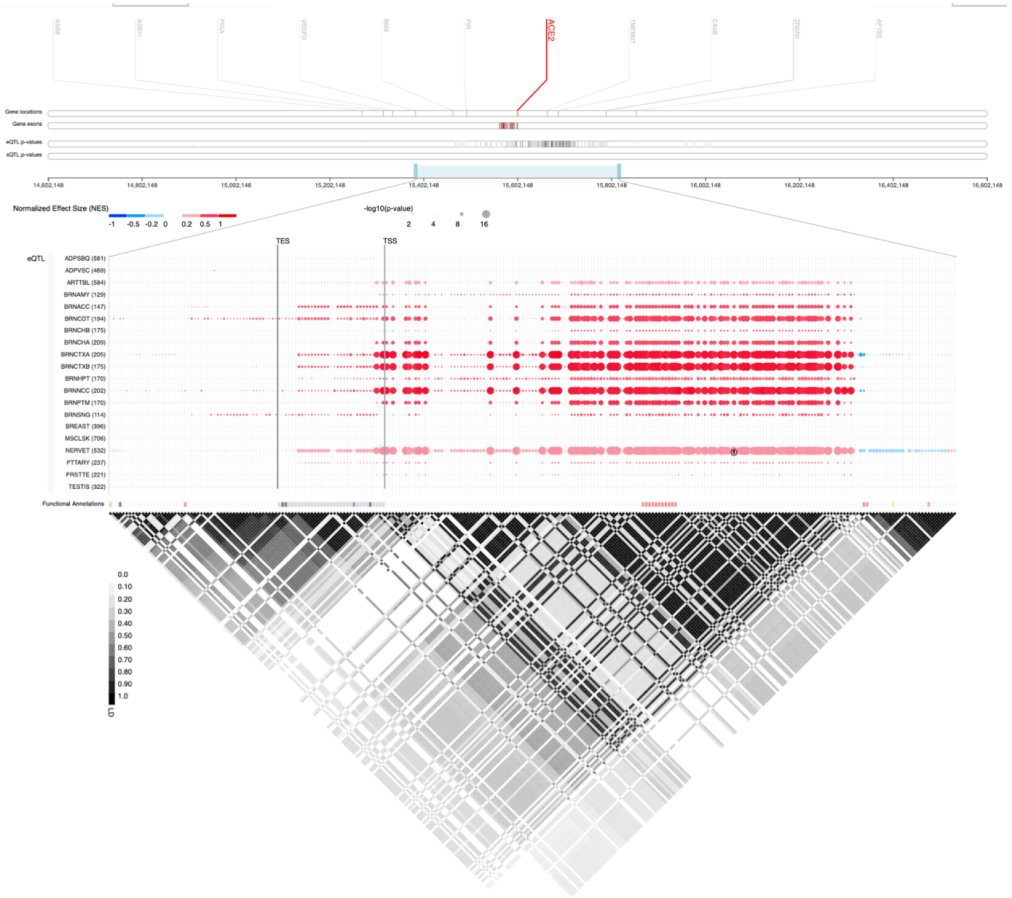

Figure 2

a

TMPRSS2 eQTLs various tissues

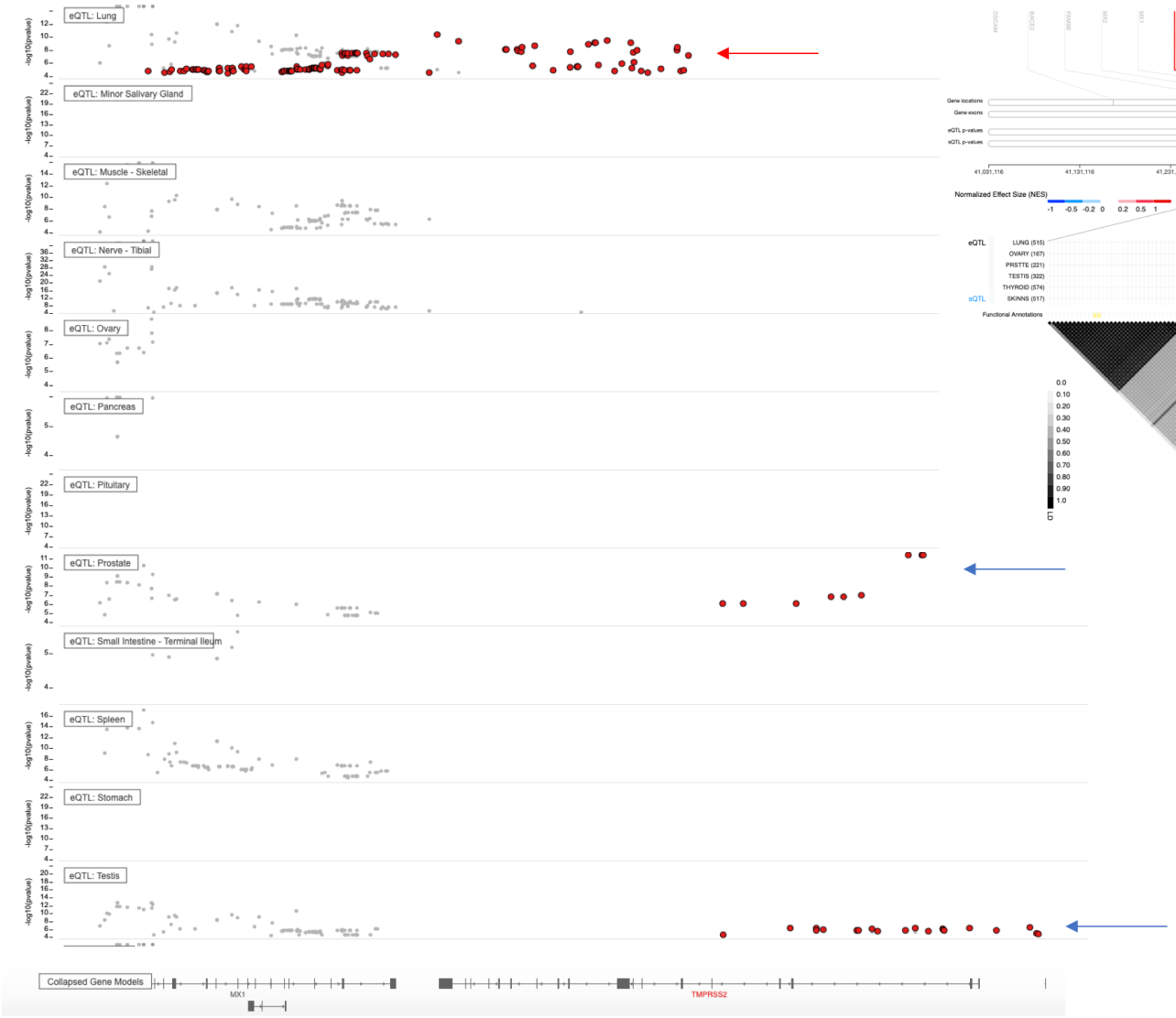

b

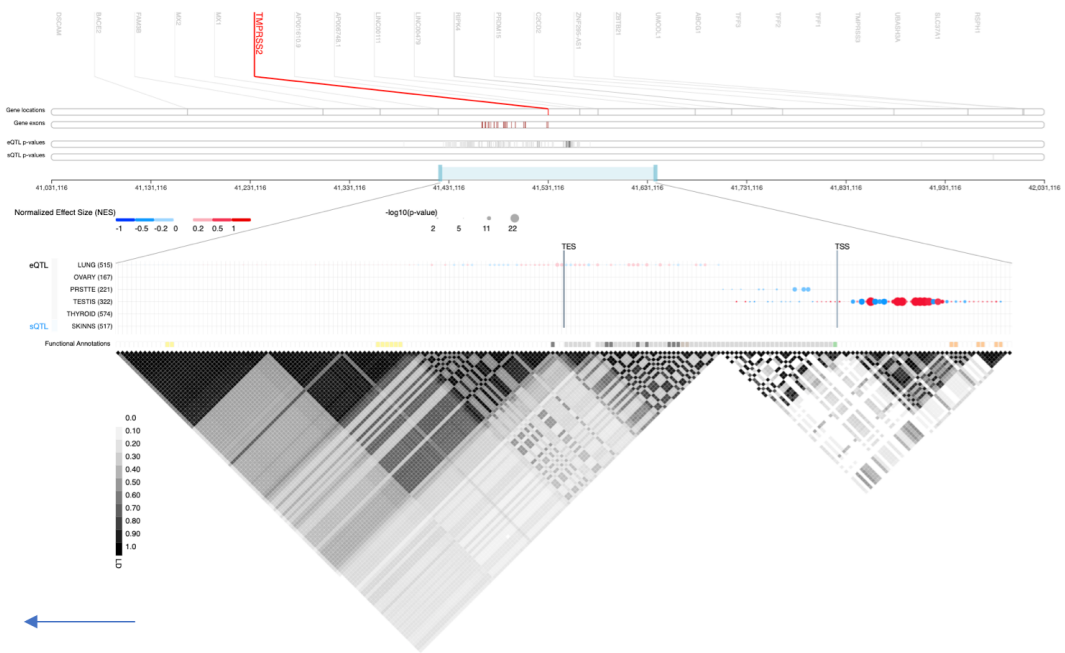

Figure 3

A.

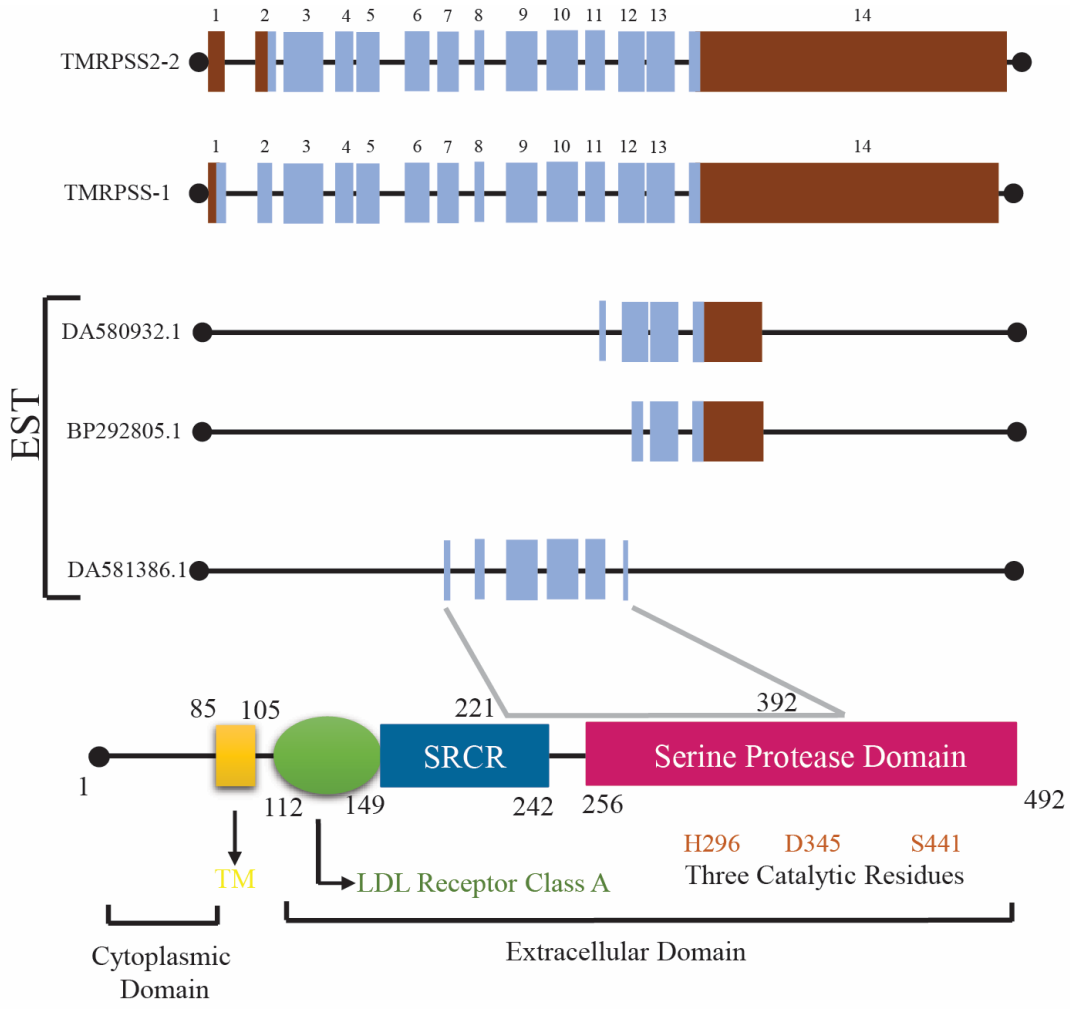
TMRPSS2-2
TMRPSS-1
1 2 3 4 5 6 7 8 9 10 11 12 13 14
EST
DA580932.1
BP292805.1
DA581386.1
85 105 221 392
1 112 149 242 256 492
SRCR
Serine Protease Domain
H296 D345 S441
Three Catalytic Residues
TM
LDL Receptor Class A
Cytoplasmic Domain
Extracellular Domain

B.

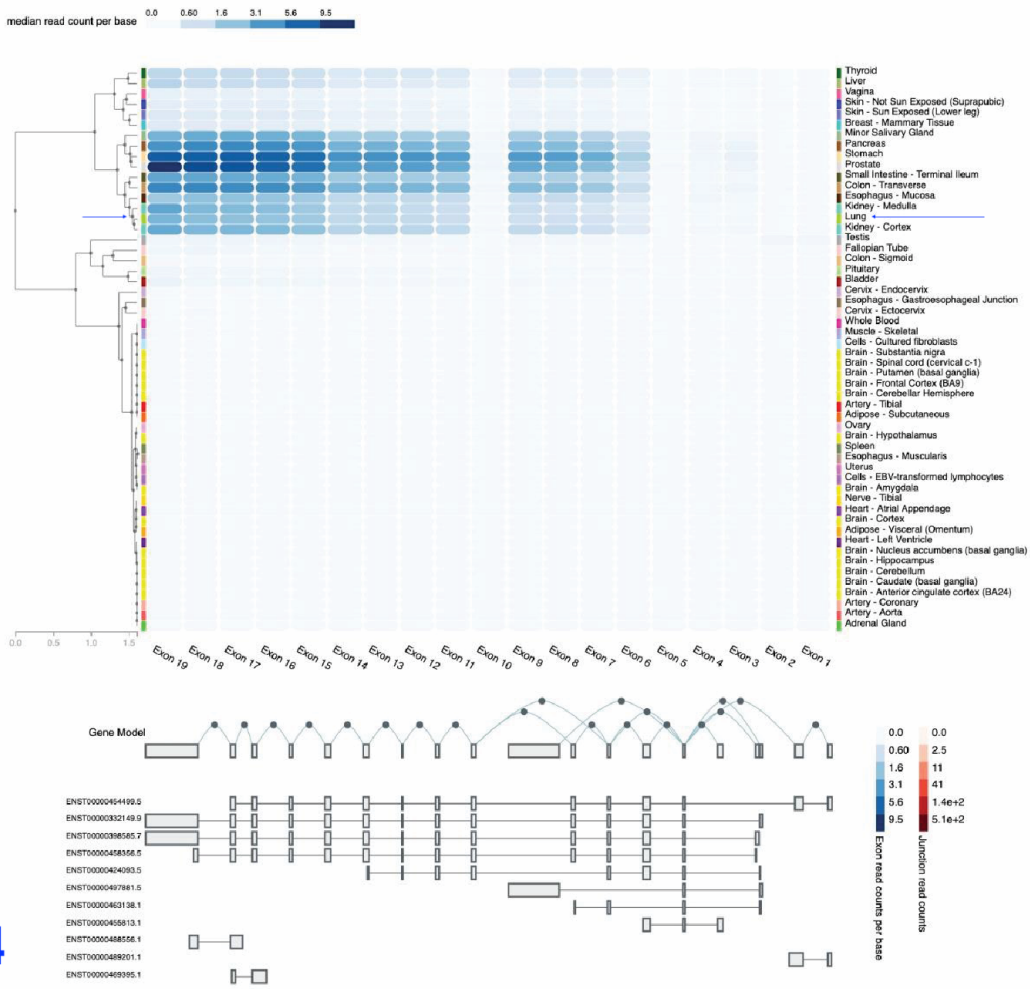
median read count per base
Gene Model
Exon read counts per base
Junction read counts

Figure 4

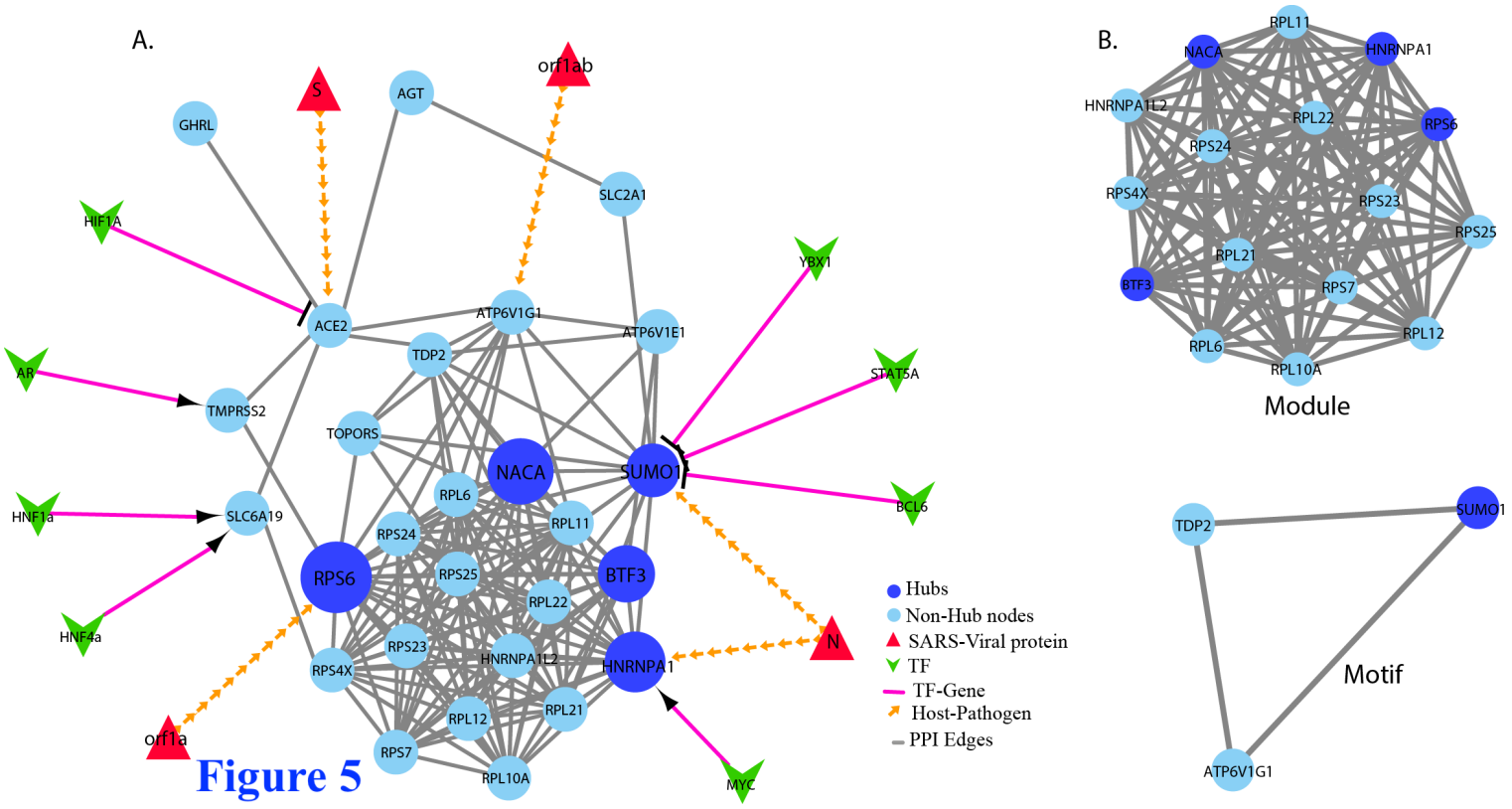
A.
S
orf1ab
AGT
GHRL
SLC2A1
HIF1A
YBX1
ACE2
ATP6V1G1
ATP6V1E1
TDP2
AR
STAT5A
TMPRSS2
TOPORS
NACA
SUMO1
BCL6
HNF1a
SLC6A19
RPL6
RPL11
RPS24
RPS6
RPS25
BTF3
RPL22
HNF4a
N
RPS23
HNRNPA1L2
HNRNPA1
RPS4X
RPL12
RPL21
orf1a
RPS7
RPL10A
MYC
Hubs
Non-Hub nodes
SARS-Viral protein
TF
TF-Gene
Host-Pathogen
PPI Edges
B.
RPL11
NACA
HNRNPA1
HNRNPA1L2
RPL22
RPS6
RPS24
RPS4X
RPS23
RPS25
RPL21
BTF3
RPS7
RPL12
RPL6
RPL10A
Module
TDP2
SUMO1
Motif
ATP6V1G1

Figure 5

Supplementary Information

ACE2 Homo-dimerization, Human Genomic variants and Interaction of Host Proteins Explain High Population Specific Differences in Outcomes of COVID19

Swarkar Sharma[1*], Inderpal Singh[2†], Shazia Haider[3†], Md. Zubbair Malik[4†], Kalaiarasan Ponnusamy[5†], Ekta Rai[1]

1. Human Genetics Research Group, School of Biotechnology, Shri Mata Vaishno Devi University, Katra, Jammu and Kashmir, India.
2. Bioinfores Pvt. Ltd., R. S. Pura, Jammu, Jammu and Kashmir, India.
3. Department of Biotechnology, Jaypee Institute of Information Technology, Noida, Sector-62, Uttar Pradesh, India
4. School of Computational and Integrative Sciences, Jawaharlal Nehru University, New Delhi, India.
5. School of Biotechnology, Jawaharlal Nehru University, New Delhi, India.

† - All authors contributed Equally

Corresponding Author:
Dr. Swarkar Sharma
Coordinator, Human Genetics Research Group,
School of Biotechnology, Shri Mata Vaishno Devi University, Katra, J&K, India
Email: swarkar.sharma@smvdu.ac.in
Mobile: +91-9419955636; Ph: +91-1991-285535//285525 Ext. 2385

Additional information about knock-out experiment in Network analysis

Perturbation by leading hub removal analysis

Degree Distribution (P(k)): Degree k is the number of interaction a node in the HPIN. *P(k)* is the probability of randomly chosen node to have k interaction with the neighbour. The probability of degree distribution *(P(k))* of the network is calculated by:

$$P(k) = \frac{n_k}{N}$$

where, n_k is equal to the number of nodes with degree k and N is equal to the size of the network (Albert and Barabási, 2002; Barabasi and Albert, 1999).

Clustering Coefficient (C(k)): Clustering coefficient defines how strongly the nodes in a network tend to cluster together. Clustering coefficient of the ith node in undirected network can be obtained by:

$$C(k_i) = \frac{2e_i}{k_i(k_i - 1)}$$

where, e_i is the number of connected pairs of the nearest-neighbour of the *i-th* node and k_i denotes the degree of the respective node (Ravasz and Barabasi, 2003; Ravasz, et al., 2002).

Neighborhood Connectivity ($C_N(k)$): Neighbourhood connectivity of a node is defined as the connectivity of all the neighbours of the node (Maslov and Sneppen, 2002). The average connectivity of the nearest neighbours of a node is given by:

$$C_N(k) = \sum_q qP(q|k)$$

where, $P(q|k)$ denotes the conditional probability that a link belonging to a node with connectivity k points to a node with connectivity q.

For scale free network, $C_N(k)$ is constant while it follows power law $C_N(k)= c^{-\mu}$ for hierarchical network with μ approximately equal to 0.5 (Pastor-Satorras, et al., 2001). The positive and negative signs in μ indicates the assortivity or disassortivity of network respectively (Barrat, et al., 2004).

References

1. Albert, R. and Barabási, A.-L. Statistical mechanics of complex networks. Reviews of Modern Physics 2002;74(1):47-97.
2. Barabasi, A.L. and Albert, R. Emergence of scaling in random networks. Science 1999;286(5439):509-512.
3. Barrat, A., et al. The architecture of complex weighted networks. Proceedings of the National Academy of Sciences of the United States of America 2004;101(11):3747-3752.
4. Maslov, S. and Sneppen, K. Specificity and stability in topology of protein networks. Science 2002;296(5569):910-913.
5. Pastor-Satorras, R., Vazquez, A. and Vespignani, A. Dynamical and correlation properties of the internet. Phys Rev Lett 2001;87(25):258701.
6. Ravasz, E. and Barabasi, A.L. Hierarchical organization in complex networks. Phys Rev E Stat Nonlin Soft Matter Phys 2003;67(2 Pt 2):026112.

7. Ravasz, E., et al. Hierarchical organization of modularity in metabolic networks. Science 2002;297(5586):1551-1555.

Supplementary figures

Figure S1. Structural representation and essential dynamics of ACE2

A multi chain complex of dimeric ACE2 is shown (colored as purple and forest green surface representation) bound to B0AT1 (colored as chocolate and orange surface) through its C terminal amino acids and SARS-CoV-2 RBD domain through its N terminal amino acids (shown as black and blue surface), the recognition site of TMPRSS2 is also highlighted as surface against the cartoon background [A]. The cartoon representation along with CPK spheres blue-white-red showing the direction of essential dynamics calculated through PCAs PC1 of ACE2-RBD region from both simulations is shown [B and C].

Figure S1'. Root mean square fluctuation and contribution of ACE2 residues to PC1 and 2 along with proportion of variance

Root mean square fluctuation (RMSF) plots of ACE2 protein from monomeric ACE2-RBD viral complex and dimeric ACE2(single chain)-RBD complex are shown. The localized fluctuation profile of the amino acids across the protein were similar for both simulation conditions except higher fluctuation in the region that constitutes the ACE2 dimerization interface and following C terminal helix which interacts with B0AT1 (B0AT1 was deleted in the monomeric ACE2-RBD simulation [A]. The contribution of the amino acids to the principal component (PC) 1 and 2 (black and red respectively) along with the scree plot reporting the proportion of variance by each PC are shown [B and C]. It can be observed that the N terminal amino acids consisting of the ACE2-RBD binding site contributed more to the overall essential dynamics in dimeric compared monomeric ACE2 simulated in the present study.

Figure S2. Expression of host genes in Lungs, alternative transcripts of *ACE2* and expression data depiction and regulatory elements and other annotations related to ACE2

(a) Expression of various human genes in Human Lungs from GTEx portal. Normalized Expression Values as Transcripts per million (TPM) are plotted as shades from yellow to deep blue in low to high order. (b) Expression levels as median read count per base as shades of blue from low to high values indicating exons expression in different tissues in GTEx portal. Gene models of alternate transcripts are also depicted. (c) Expression levels as median read count per base as shades of red from low to high values indicating exons junctions expression in different tissues in GTEx portal. (d) UCSC genome browser showing various tracks at 5' Untranslated region of ACE2 gene, common dbSNPs 153 intersecting with conserved transcription factors and conserved transcription factor binding sites are also depicted.

Figure S3 The screenshot from Human Protein Atlas depicting Human ACE2 expression

RNA and Protein expression in different tissues is depicted. In lungs, only RNA expression of ACE2 gene is shown with no ACE2 protein expression.

Figure S4. Annotation of *ACE2* depicting various regulatory elements in UCSC Genome browser

UCSC genome browser showing SNPs rs1978124 and rs2106809 in intron 1 of ACE2 gene. Various tracks covering first 2 exons and 5' Untranslated region of ACE2 gene are shown. The ACE2 gene is located on negative strand. In the region GH0XJ015596 enhancer (in red colour) can be located in the track Enhancer and promoter from GeneHancer database.

Figure S5. Frequency distribution of SNPs rs1978124 and rs2106809 in 1000G population groups

Frequency distribution of SNPs, rs1978124 and rs2106809 in 1000G populations dataset, also depicted on world map by a web based tool Datawrapper (https://www.datawrapper.de/). Derived allele frequencies in both the SNPs are also plotted for comparison, indicating differential frequency distribution in different population groups. SNPs showed relatively uniform frequency distribution trend in sub populations belonging to same super population groups EUR and EAS. However, differences can be seen amongst the AFR, AMR and SAS sub population groups.

Figure S6. UCSC Genome browser screenshot depicting proxy SNPs and LD structure in the *ACE2* region

UCSC genome browser showing r^2 plot along with other annotations for SNPs rs1978124 and rs2106809 from the intron 1 of ACE2 gene. GeneHancer regulator elements and interaction between GeneHancer regulatory elements as curved lines can be seen. In addition, it can be seen that all the proxy SNPs (in Brown) are clustered together within potential functional regulatory enhancer element and interaction region (in brown color).

Figure S7. Expression of TMPRSS2 in different tissues

(a) Expression of TMPRSS2 in different tissues as reterived from GTEx portal. Transcripts per million (TPM) are plotted on Y axis and different tissues on X axis. (b) RNA and Protein expression in different tissues is depicted in Human Protein Atlas online portal. In lungs, only RNA expression of TMPRSS2 gene is noted with no protein expression depiction. (c) Expression levels as read count in shades of purple from low to high values indicating expression of different transcripts in different tissues in GTEx portal. Gene models of alternate transcripts are also depicted.

Figure S8. UCSC Genome browser screenshot depicting Lung eQTLs along with SNPs and LD structure in the *TMPRSS2* region

Lung eQTLs that overlapped with the common dbSNPs are shown and along r^2 values depicting LD in the region is plotted. All the SNPs appeared to cluster towards 3' end of the gene. Other annotations include GeneHancer regulator elements and interaction between GeneHancer regulatory elements as curved lines can be seen. (dark blue color for TMPRSS2 gene). Alternate splicing graph is also indicated.

Figure S9. Elucidation of key functional SNPs of *TMPRSS2* and their Frequency distribution in 1000G population groups

(a) TMPRSS2 gene eQTLs in lungs appear to cluster in the gene towards 3' end and potentially are associated with expression of alternative transcripts in lungs. (b) Amongst these common eQTLs, HaploReg annotations indicated rs4818239 as an important SNP. (c) Frequency distribution on world map of rs4818239
(d) rs75603675 (p.Gly8Val) (e) rs12329760 (p.Val197Met)
The frequencies of SNPs are based on 1000G populations dataset and depicted on world map by LDpop tool of web based LDlink 4.0.3 suite from National Cancer Institute, USA. Derived allele frequencies from low to high are plotted as shades of white to blue.

Figure S10. Sequence alignment and structure of TMPRSS2

(A) The pairwise sequence alignment shows the N-terminal difference in two isoforms and highlights two mutation regions. (B) The predicted 3D structure of TMPRSS2 protein. Two domains of TMPRSS2 and mutation residue are highlighted in the carton model with different colors.

Figure S11. *In silico* protein-protein docking analysis of TMPRSS2.

(A1) Surface Model (A2) Carton Model of TMPRSS2 (Pink) human protein interaction with ACE2 (Green) of SARS CoV-2. (B1) Surface Model (B2) Carton Model of Docked complex of SARS CoV-2 S-protein protein (Blue) with TMPRSS2 (Pink). (C) Comparison of docking score between wild-type and mutant TMPRSS2 with ACE2 and SARS CoV-2 S-protein.

Figure S12. Summarised information about SLC6A19 gene and its variants

(a) Expression of TMPRSS2 in different tissues as retrieved from GTEx portal indicates very restricted expression of the gene. Expression levels as read count in shades of purple from low to high values. Gene models of alternate transcripts are also depicted.(b) Expression levels as median read count per base as shades of blue from low to high values indicating exons expression in different tissues in GTEx portal. Gene models of alternate transcripts are also depicted. (c) SLC6A19 RNA and Protein expression in different tissues is depicted in Human Protein Atlas online portal indicating SLC6A19 has very restricted expression in tissues and in lungs neither its RNA nor Protein expresses. (d) UCSC genome browser screenshot highlights a prominent Enhancer element GH05J001199 at 5'UTR of the gene overlapping exon 1 and extending in intron 1 of the gene. (e) Screenshot from UCSC genome browser depicting SNPs cluster overlapping and

intersecting enhancer region GH05J001199. It also depicts common variants (with applied filter on track for SNPs with frequency greater than 20 percent in global populations) in dbSNP version 151. (f) eQTLs in different tissues for *SLC6A19* were plotted through GTEx Locus Browser. Size of the dot indicate level of significance (as negative p values) whereas colour depicts positive or negative correlation with Normalized effect size (NES) of the eQTL from -1 to 0 to 1. Red color shades represent upregulation whereas blue color shades show downregulation. It also depicts Linkage disequilibrium (LD) in region with value range from 0 to 1 as white to black shades with 1(dark) as absolute LD. Significant upregulation of the gene by eQTLs was observed in Pancreas whereas downregulation in Liver and no data on Lungs as it is reported not to be expressing in Lungs at GTEx portal.

Figure S13. Number of diseases associated with hub proteins.

(A) The network view where nodes represent diseases and hub proteins and edges the association between them. (All the nodes of diseases rectangle (red), diseases highly associated with hub proteins rectangle (light green) and hub proteins circle (cyan) are filled color and edges in lines (grey).

(B) The pie chart graph showing the percentage distribution of each hub proteins associated with diseases.

Figure S14. Topological characteristics of the HPIN and hub removal.

(A) The figure illustrates the network properties, such as in-degree, out-degree, clustering coefficient, neighbourhood connectivity in the HPIN. The In-degree ($P(k)_{In}$) and out-degree ($P(k)_{out}$) distribution, Clustering Co-efficient C(k), Neighbourhood connectivity $C_N(k)$ is fitted to the power law distribution with exponent values (α, β, γ & μ).

(B) Power law distribution with exponent values α, β, γ & μ of HPIN (complete), hub removed proteins network (RPS6, NACA, HNRNPA1 and BTF3*)*.

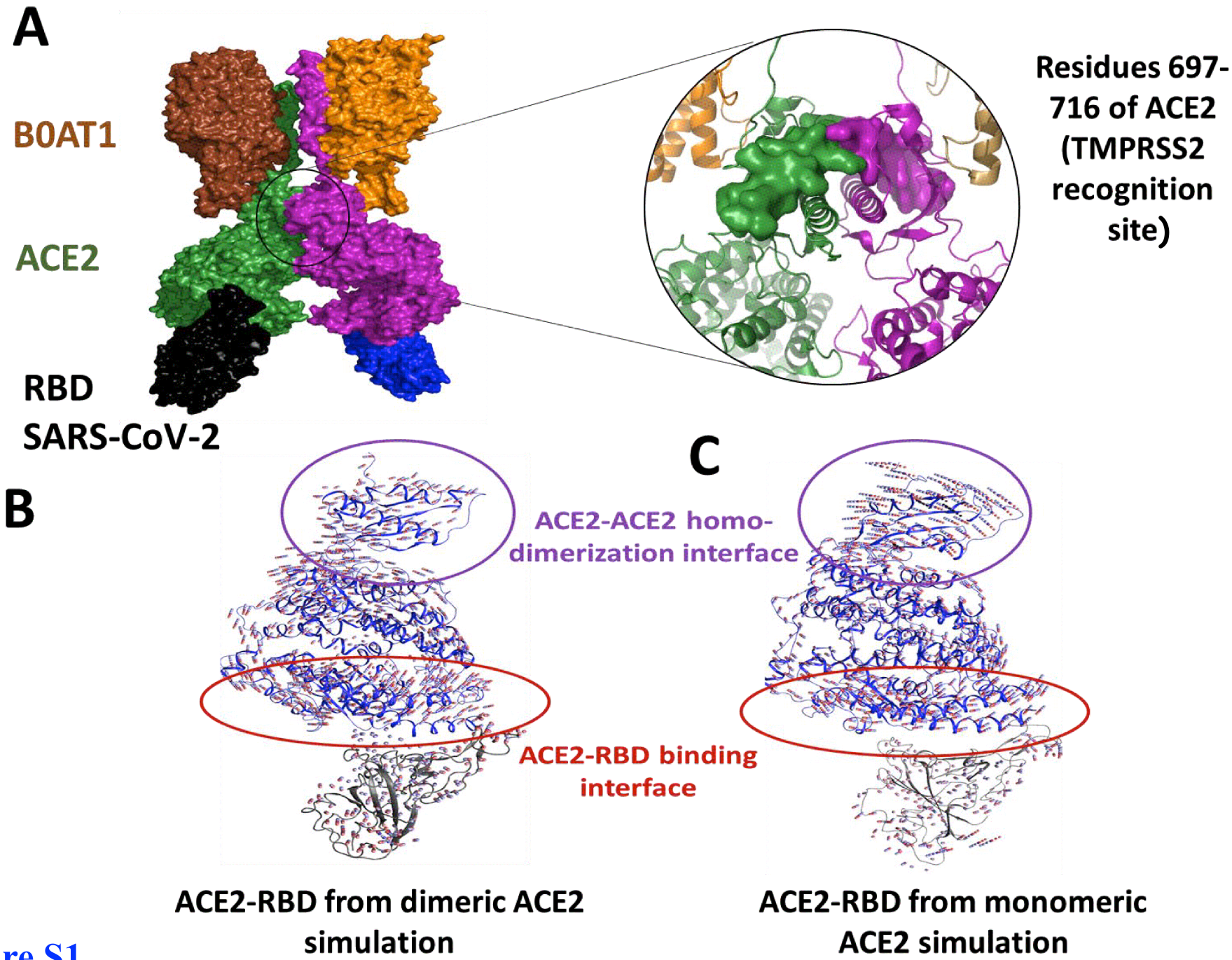
A
B0AT1
ACE2
RBD
SARS-CoV-2
Residues 697-716 of ACE2 (TMPRSS2 recognition site)
B
C
ACE2-ACE2 homo-dimerization interface
ACE2-RBD binding interface
ACE2-RBD from dimeric ACE2 simulation
ACE2-RBD from monomeric ACE2 simulation

Figure S1

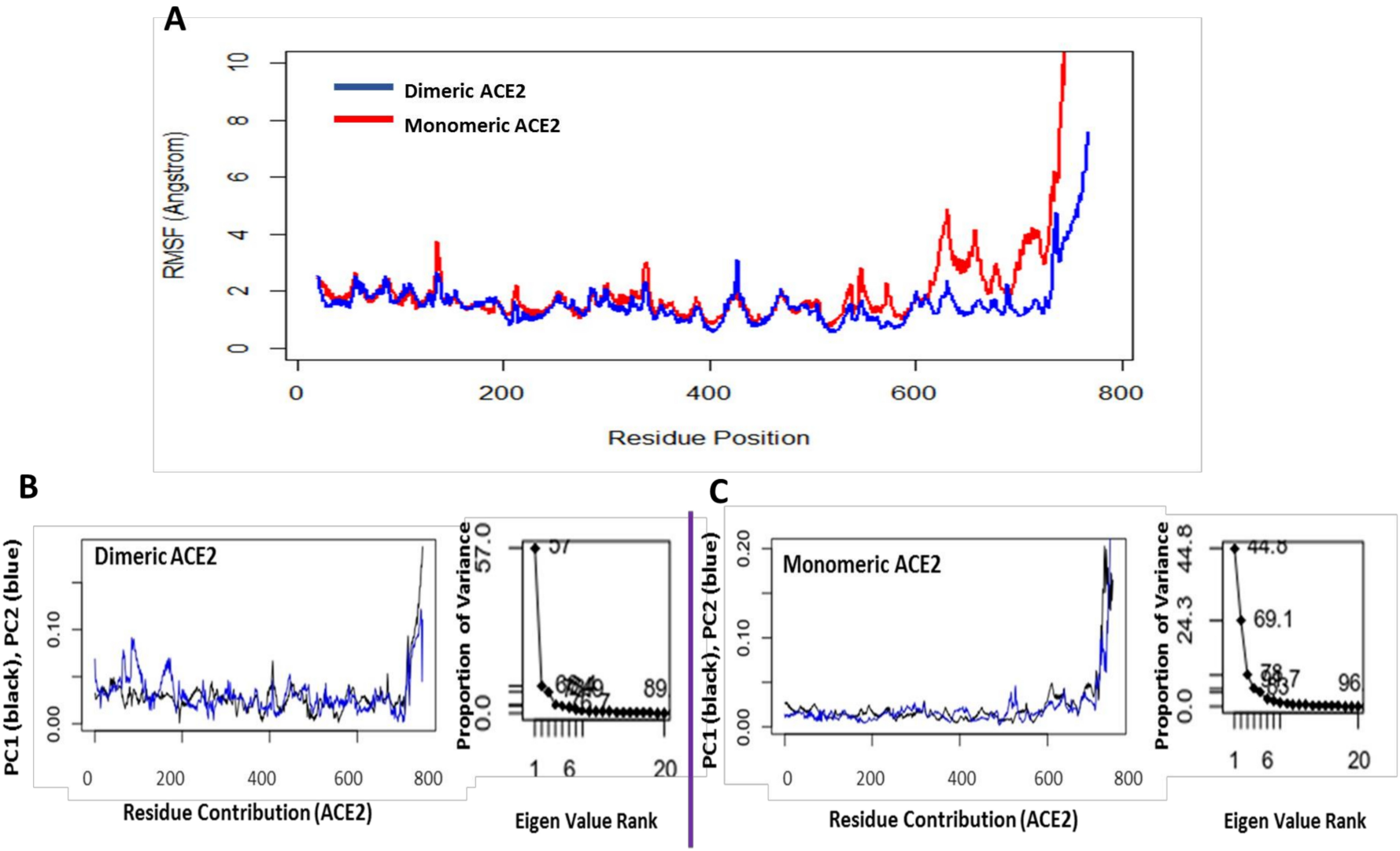
A
Dimeric ACE2
Monomeric ACE2
RMSF (Angstrom)
Residue Position
B
Dimeric ACE2
PC1 (black), PC2 (blue)
Residue Contribution (ACE2)
Proportion of Variance
Eigen Value Rank
C
Monomeric ACE2
PC1 (black), PC2 (blue)
Residue Contribution (ACE2)
Proportion of Variance
Eigen Value Rank

Figure S1”

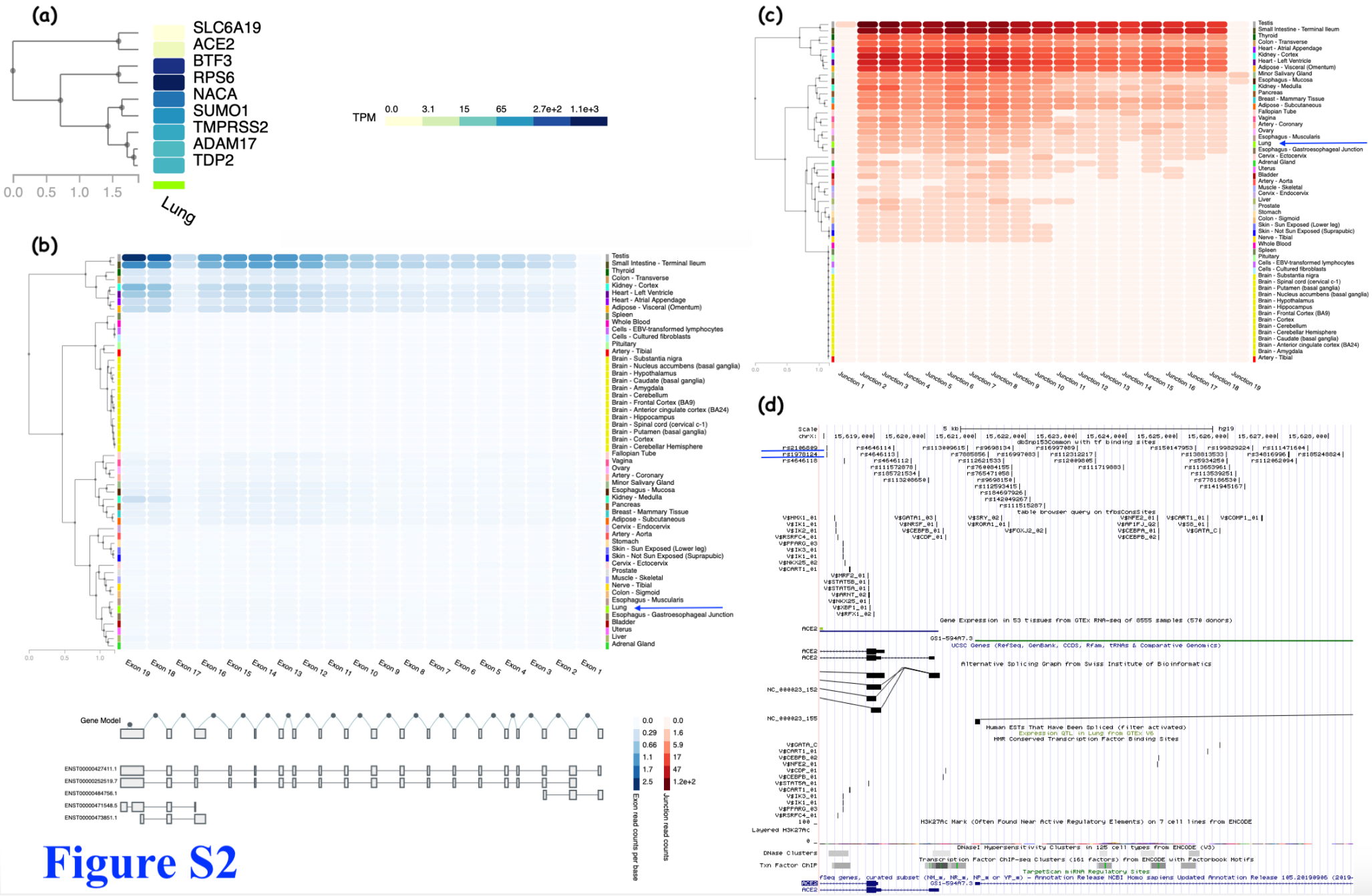
(a)
SLC6A19
ACE2
BTF3
RPS6
NACA
SUMO1
TMPRSS2
ADAM17
TDP2
Lung
0.0 0.5 1.0 1.5
TPM 0.0 3.1 15 65 2.7e+2 1.1e+3
(b)
Testis
Small Intestine - Terminal Ileum
Thyroid
Colon - Transverse
Kidney - Cortex
Heart - Left Ventricle
Heart - Atrial Appendage
Adipose - Visceral (Omentum)
Spleen
Whole Blood
Cells - EBV-transformed lymphocytes
Cells - Cultured fibroblasts
Pituitary
Artery - Tibial
Brain - Substantia nigra
Brain - Nucleus accumbens (basal ganglia)
Brain - Hypothalamus
Brain - Caudate (basal ganglia)
Brain - Amygdala
Brain - Cerebellum
Brain - Frontal Cortex (BA9)
Brain - Anterior cingulate cortex (BA24)
Brain - Hippocampus
Brain - Spinal cord (cervical c-1)
Brain - Putamen (basal ganglia)
Brain - Cortex
Brain - Cerebellar Hemisphere
Fallopian Tube
Vagina
Ovary
Artery - Coronary
Minor Salivary Gland
Esophagus - Mucosa
Kidney - Medulla
Pancreas
Breast - Mammary Tissue
Adipose - Subcutaneous
Cervix - Endocervix
Artery - Aorta
Stomach
Skin - Sun Exposed (Lower leg)
Skin - Not Sun Exposed (Suprapubic)
Cervix - Ectocervix
Prostate
Muscle - Skeletal
Nerve - Tibial
Colon - Sigmoid
Esophagus - Muscularis
Lung
Esophagus - Gastroesophageal Junction
Bladder
Uterus
Liver
Adrenal Gland
0.0 0.5 1.0
Exon 19 Exon 18 Exon 17 Exon 16 Exon 15 Exon 14 Exon 13 Exon 12 Exon 11 Exon 10 Exon 9 Exon 8 Exon 7 Exon 6 Exon 5 Exon 4 Exon 3 Exon 2 Exon 1
Gene Model
ENST00000427411.1
ENST00000252519.7
ENST00000484756.1
ENST00000471548.5
ENST00000473851.1
0.0 0.29 0.66 1.1 1.7 2.5
Exon read counts per base
0.0 1.6 5.9 17 47 1.2e+2
Junction read counts
(c)
Testis
Small Intestine - Terminal Ileum
Thyroid
Colon - Transverse
Heart - Atrial Appendage
Kidney - Cortex
Heart - Left Ventricle
Adipose - Visceral (Omentum)
Minor Salivary Gland
Esophagus - Mucosa
Kidney - Medulla
Pancreas
Breast - Mammary Tissue
Adipose - Subcutaneous
Fallopian Tube
Vagina
Artery - Coronary
Ovary
Esophagus - Muscularis
Lung
Esophagus - Gastroesophageal Junction
Cervix - Ectocervix
Adrenal Gland
Uterus
Bladder
Artery - Aorta
Muscle - Skeletal
Cervix - Endocervix
Liver
Prostate
Stomach
Colon - Sigmoid
Skin - Sun Exposed (Lower leg)
Skin - Not Sun Exposed (Suprapubic)
Nerve - Tibial
Whole Blood
Spleen
Pituitary
Cells - EBV-transformed lymphocytes
Cells - Cultured fibroblasts
Brain - Substantia nigra
Brain - Spinal cord (cervical c-1)
Brain - Putamen (basal ganglia)
Brain - Nucleus accumbens (basal ganglia)
Brain - Hypothalamus
Brain - Hippocampus
Brain - Frontal Cortex (BA9)
Brain - Cortex
Brain - Cerebellum
Brain - Cerebellar Hemisphere
Brain - Caudate (basal ganglia)
Brain - Anterior cingulate cortex (BA24)
Brain - Amygdala
Artery - Tibial
0.0 0.5 1.0
Junction 1 Junction 2 Junction 3 Junction 4 Junction 5 Junction 6 Junction 7 Junction 8 Junction 9 Junction 10 Junction 11 Junction 12 Junction 13 Junction 14 Junction 15 Junction 16 Junction 17 Junction 18 Junction 19
(d)
Scale
chrX:
hg19
Gene Expression in 53 tissues from GTEx RNA-seq of 8555 samples (570 donors)
ACE2
GS1-594A7.3
UCSC Genes (RefSeq, GenBank, CCDS, Rfam, tRNAs & Comparative Genomics)
Alternative Splicing Graph from Swiss Institute of Bioinformatics
NC_000023_152
NC_000023_155
Human ESTs That Have Been Spliced (filter activated)
Expression QTL in Lung from GTEx V6
HMR Conserved Transcription Factor Binding Sites
H3K27Ac Mark (Often Found Near Active Regulatory Elements) on 7 cell lines from ENCODE
Layered H3K27Ac
DNaseI Hypersensitivity Clusters in 125 cell types from ENCODE (V3)
DNase Clusters
Transcription Factor ChIP-seq Clusters (161 factors) from ENCODE with Factorbook Motifs
Txn Factor ChIP
TargetScan miRNA Regulatory Sites

Figure S2

ACE2

THE HUMAN PROTEIN ATLAS

MENU HELP NEWS

ace2 Search

TISSUE ATLAS

PRIMARY DATA

GENE/PROTEIN

ANTIBODIES AND VALIDATION

Dictionary

Tissue proteome

RNA AND PROTEIN EXPRESSION SUMMARY[i]

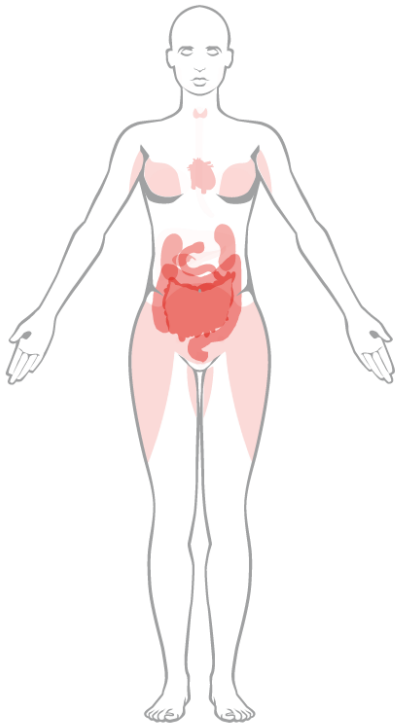

Expression Detection All organs

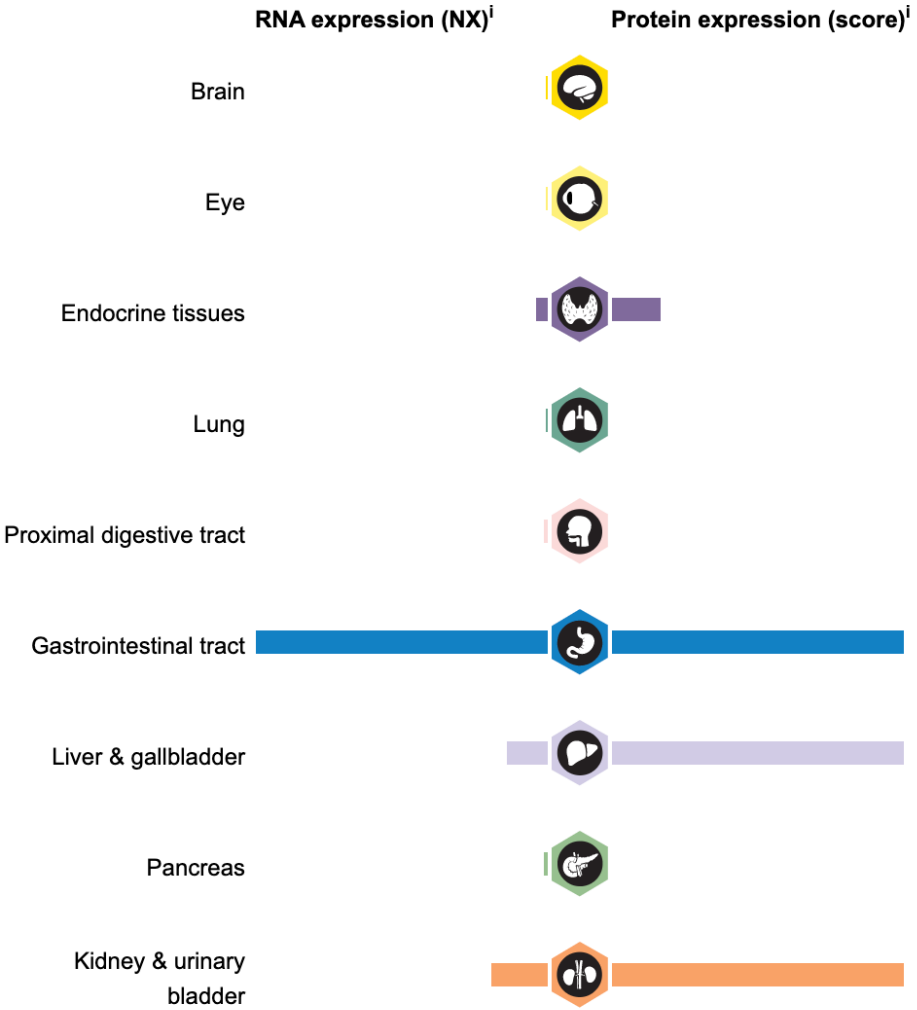

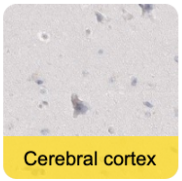

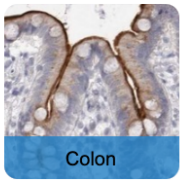

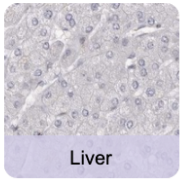

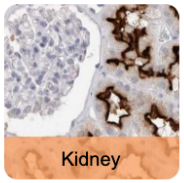

Figure S3

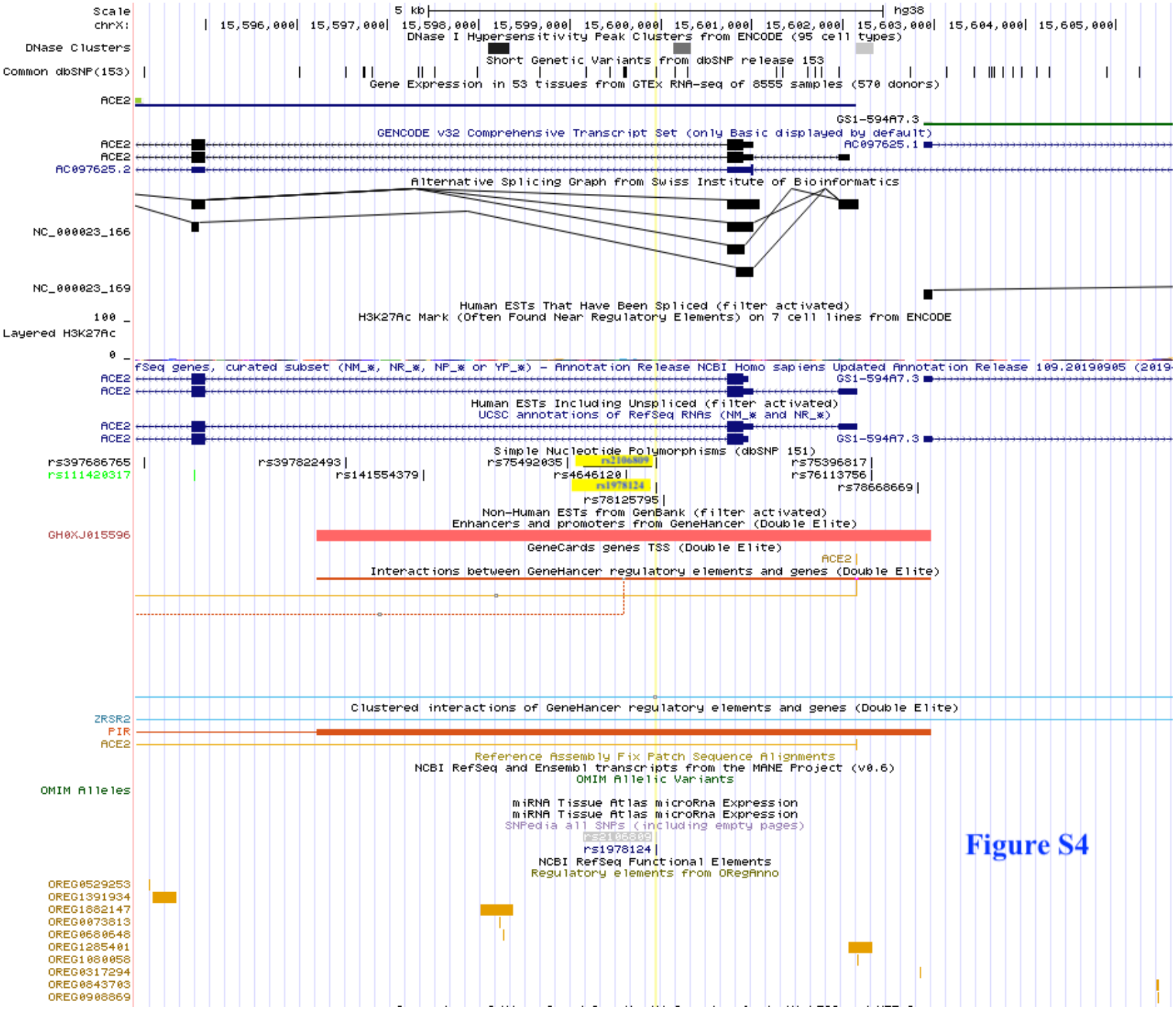
Scale
chrX:
5 kb
hg38
15,596,000
15,597,000
15,598,000
15,599,000
15,600,000
15,601,000
15,602,000
15,603,000
15,604,000
15,605,000
DNase Clusters
DNase I Hypersensitivity Peak Clusters from ENCODE (95 cell types)
Common dbSNP(153)
Short Genetic Variants from dbSNP release 153
Gene Expression in 53 tissues from GTEx RNA-seq of 8555 samples (570 donors)
ACE2
GS1-594A7.3
GENCODE v32 Comprehensive Transcript Set (only Basic displayed by default)
AC097625.1
AC097625.2
Alternative Splicing Graph from Swiss Institute of Bioinformatics
NC_000023_166
NC_000023_169
Human ESTs That Have Been Spliced (filter activated)
100
H3K27Ac Mark (Often Found Near Regulatory Elements) on 7 cell lines from ENCODE
Layered H3K27Ac
0
fSeq genes, curated subset (NM_*, NR_*, NP_* or YP_*) - Annotation Release NCBI Homo sapiens Updated Annotation Release 109.20190905 (2019
Human ESTs Including Unspliced (filter activated)
UCSC annotations of RefSeq RNAs (NM_* and NR_*)
Simple Nucleotide Polymorphisms (dbSNP 151)
rs397686765
rs397822493
rs75492035
rs75396817
rs111420317
rs141554379
rs4646120
rs76113756
rs1978124
rs78668669
rs78125795
Non-Human ESTs from GenBank (filter activated)
Enhancers and promoters from GeneHancer (Double Elite)
GH0XJ015596
GeneCards genes TSS (Double Elite)
Interactions between GeneHancer regulatory elements and genes (Double Elite)
Clustered interactions of GeneHancer regulatory elements and genes (Double Elite)
ZRSR2
PIR
Reference Assembly Fix Patch Sequence Alignments
NCBI RefSeq and Ensembl transcripts from the MANE Project (v0.6)
OMIM Alleles
OMIM Allelic Variants
miRNA Tissue Atlas microRna Expression
miRNA Tissue Atlas microRna Expression
SNPedia all SNPs (including empty pages)
NCBI RefSeq Functional Elements
Regulatory elements from ORegAnno
OREG0529253
OREG1391934
OREG1882147
OREG0073813
OREG0680648
OREG1285401
OREG1080058
OREG0317294
OREG0843703
OREG0908869

Figure S4

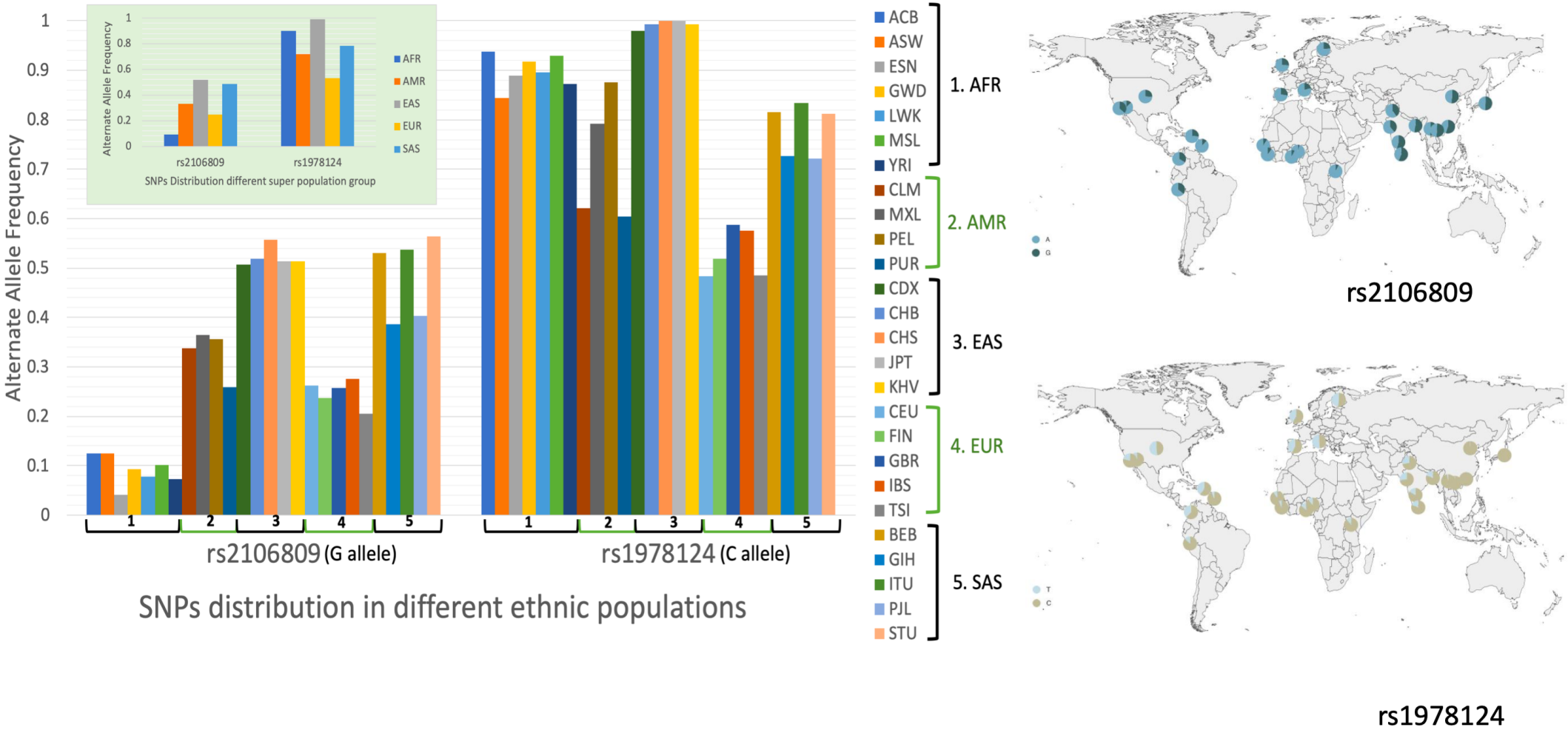
Alternate Allele Frequency
1
0.9
0.8
0.7
0.6
0.5
0.4
0.3
0.2
0.1
0
Alternate Allele Frequency
rs2106809
rs1978124
SNPs Distribution different super population group
AFR
AMR
EAS
EUR
SAS
1
2
3
4
5
rs2106809 (G allele)
rs1978124 (C allele)
SNPs distribution in different ethnic populations
ACB
ASW
ESN
GWD
LWK
MSL
YRI
CLM
MXL
PEL
PUR
CDX
CHB
CHS
JPT
KHV
CEU
FIN
GBR
IBS
TSI
BEB
GIH
ITU
PJL
STU
1. AFR
2. AMR
3. EAS
4. EUR
5. SAS
rs2106809
rs1978124

Figure S5

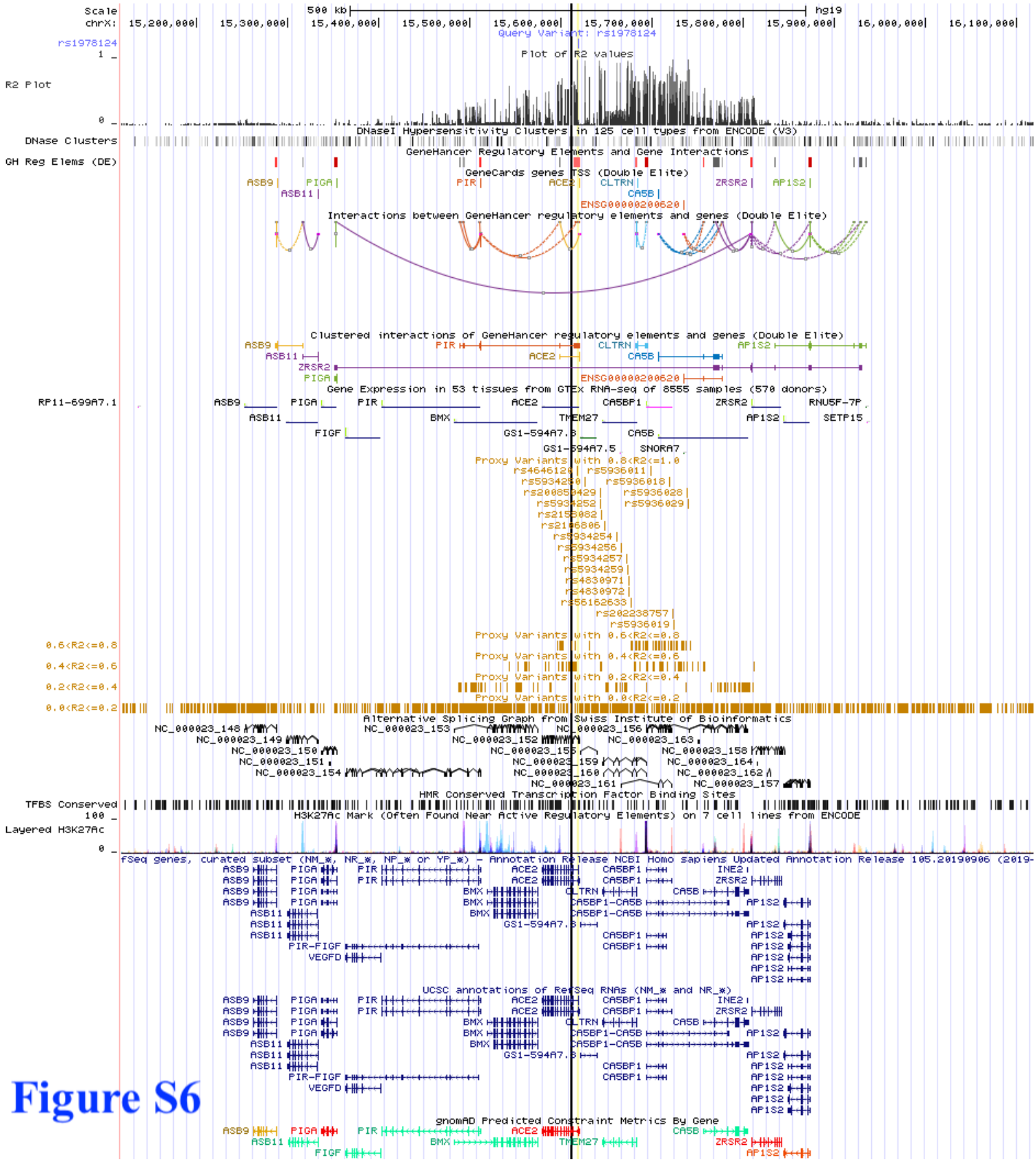
Scale
chrX:
500 kb
hg19
15,200,000
15,300,000
15,400,000
15,500,000
15,600,000
15,700,000
15,800,000
15,900,000
16,000,000
16,100,000
Query Variant: rs1978124
rs1978124
Plot of R2 values
R2 Plot
DNaseI Hypersensitivity Clusters in 125 cell types from ENCODE (V3)
DNase Clusters
GeneHancer Regulatory Elements and Gene Interactions
GH Reg Elems (DE)
GeneCards genes TSS (Double Elite)
ASB9
PIGA
ASB11
PIR
ACE2
CLTRN
CA5B
ZRSR2
AP1S2
ENSG00000200620
Interactions between GeneHancer regulatory elements and genes (Double Elite)
Clustered interactions of GeneHancer regulatory elements and genes (Double Elite)
Gene Expression in 53 tissues from GTEx RNA-seq of 8555 samples (570 donors)
RP11-699A7.1
CA5BP1
RNU5F-7P
BMX
TMEM27
SETP15
FIGF
GS1-594A7.3
GS1-594A7.5
SNORA7
Proxy Variants with 0.8<R2<=1.0
Proxy Variants with 0.6<R2<=0.8
Proxy Variants with 0.4<R2<=0.6
Proxy Variants with 0.2<R2<=0.4
Proxy Variants with 0.0<R2<=0.2
0.6<R2<=0.8
0.4<R2<=0.6
0.2<R2<=0.4
0.0<R2<=0.2
Alternative Splicing Graph from Swiss Institute of Bioinformatics
TFBS Conserved
HMR Conserved Transcription Factor Binding Sites
H3K27Ac Mark (Often Found Near Active Regulatory Elements) on 7 cell lines from ENCODE
Layered H3K27Ac
fSeq genes, curated subset (NM_*, NR_*, NP_* or YP_*) - Annotation Release NCBI Homo sapiens Updated Annotation Release 105.20190906 (2019-
PIR-FIGF
VEGFD
UCSC annotations of RefSeq RNAs (NM_* and NR_*)
gnomAD Predicted Constraint Metrics By Gene

Figure S6

a

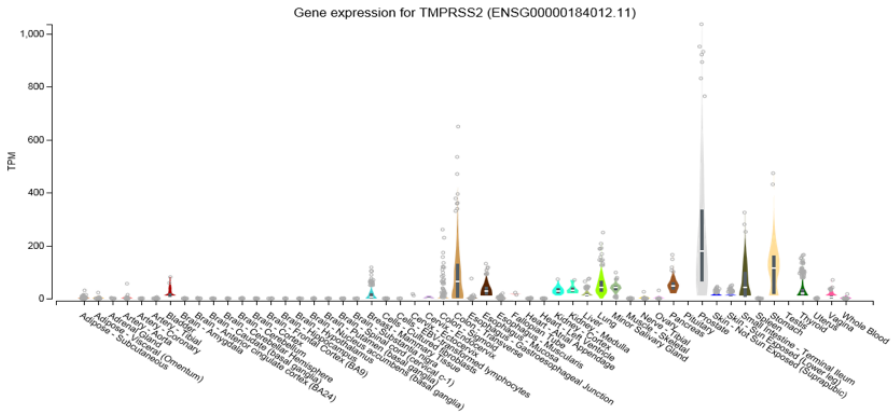

b

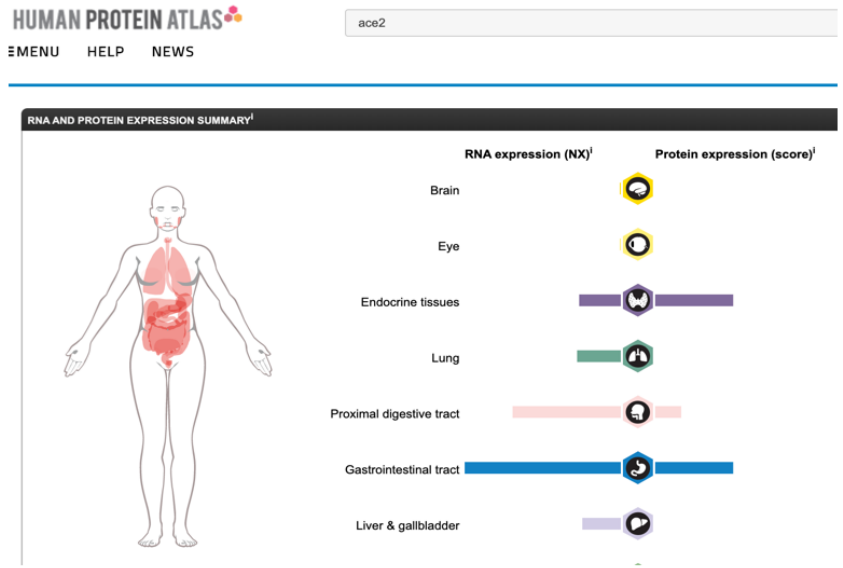

c

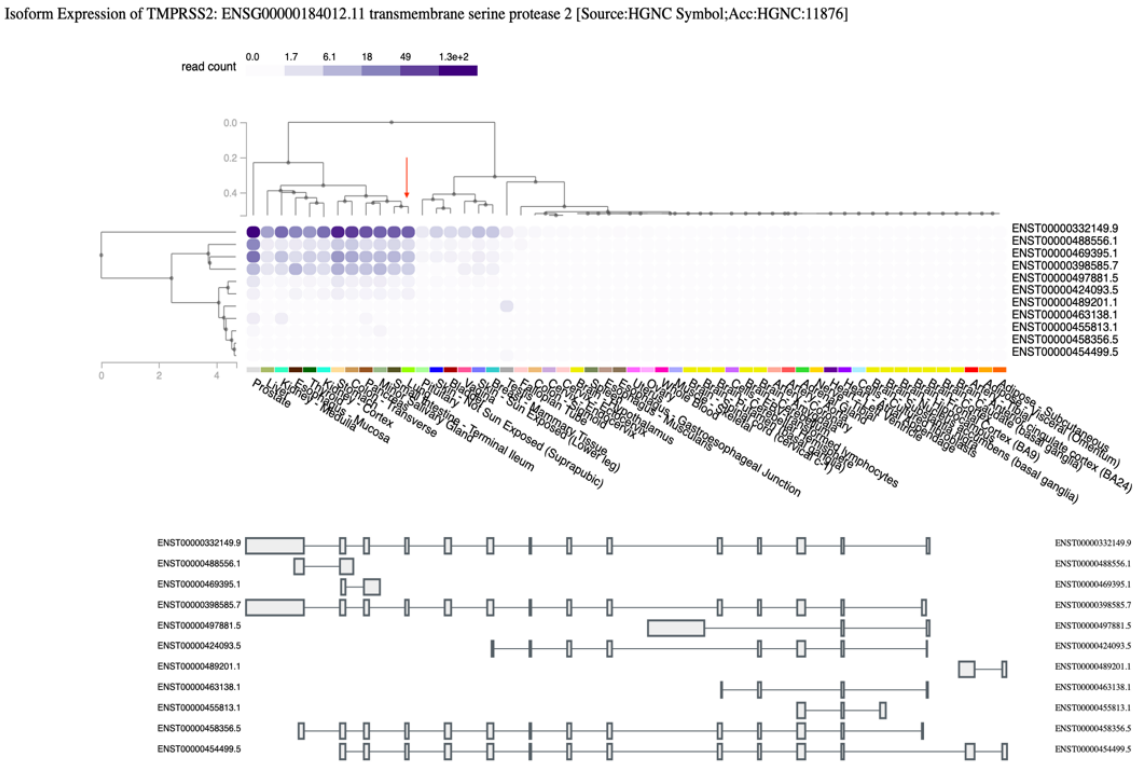

Figure S7

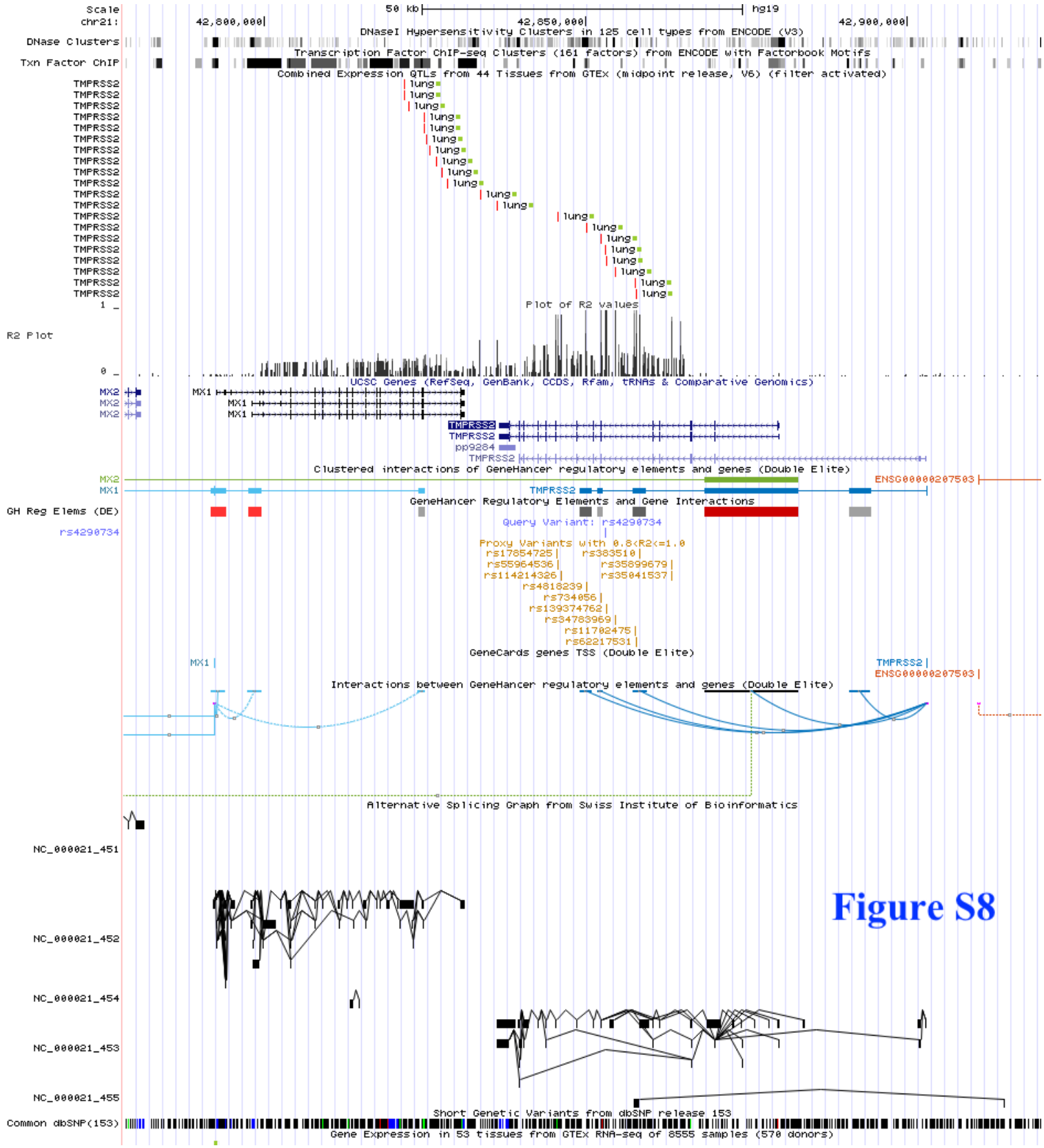
Scale
chr21:
50 kb
hg19
42,800,000
42,850,000
42,900,000
DNase Clusters
DNaseI Hypersensitivity Clusters in 125 cell types from ENCODE (V3)
Txn Factor ChIP
Transcription Factor ChIP-seq Clusters (161 factors) from ENCODE with Factorbook Motifs
Combined Expression QTLs from 44 Tissues from GTEx (midpoint release, V6) (filter activated)
TMPRSS2
lung
Plot of R2 values
R2 Plot
UCSC Genes (RefSeq, GenBank, CCDS, Rfam, tRNAs & Comparative Genomics)
MX2
MX1
TMPRSS2
pp9284
Clustered interactions of GeneHancer regulatory elements and genes (Double Elite)
ENSG00000207503
GH Reg Elems (DE)
GeneHancer Regulatory Elements and Gene Interactions
rs4290734
Query Variant: rs4290734
Proxy Variants with 0.8<R2<=1.0
rs17854725
rs383510
rs55964536
rs35899679
rs114214326
rs35041537
rs4818239
rs734056
rs139374762
rs34783969
rs11702475
rs62217531
GeneCards genes TSS (Double Elite)
Interactions between GeneHancer regulatory elements and genes (Double Elite)
Alternative Splicing Graph from Swiss Institute of Bioinformatics
NC_000021_451
NC_000021_452
NC_000021_454
NC_000021_453
NC_000021_455
Short Genetic Variants from dbSNP release 153
Common dbSNP(153)
Gene Expression in 53 tissues from GTEx RNA-seq of 8555 samples (570 donors)

Figure S8

a

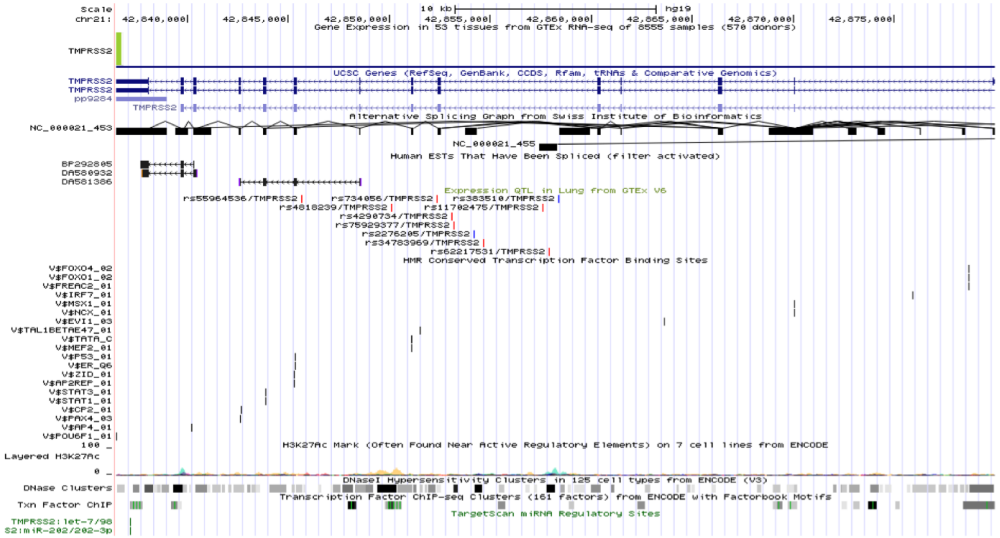

b

Query SNP: rs4818239 and variants with r^2 >= 0.8

chr	pos (hg38)	LD (r^2)	LD (D')	variant	Ref	Alt	AFR freq	AMR freq	ASN freq	EUR freq	SiPhy cons	Promoter histone marks	Enhancer histone marks	DNAse	Proteins bound	Motifs changed	NHGRI/EBI GWAS hits	GRASP QTL hits	Selected eQTL hits	GENCODE genes	dbSNP func annot
21	41478148	1	1	rs4818239	T	C	0.25	0.35	0.01	0.48		BRST, PLCNT	21 tissues	18 tissues	9 bound proteins	4 altered motifs			1 hit	TMPRSS2	intronic
21	41480393	0.93	0.97	rs734056	C	A	0.22	0.33	0.00	0.48			8 tissues	PANC,GI		Gfi1			3 hits	TMPRSS2	intronic
21	41481156	0.93	0.97	rs4290734	A	G	0.09	0.32	0.00	0.48			4 tissues	ESDR,BRN		5 altered motifs			3 hits	TMPRSS2	intronic
21	41481267	0.93	0.97	rs139374762	7-mer	T	0.13	0.32	0.00	0.48			4 tissues	5 tissues						TMPRSS2	intronic
21	41482711	0.92	0.97	rs34783969	A	T	0.14	0.33	0.00	0.48			8 tissues	6 tissues		5 altered motifs			1 hit	TMPRSS2	intronic
21	41485974	0.8	0.93	rs62217531	C	T	0.31	0.33	0.00	0.46			19 tissues	8 tissues		MZF1::1-4,THAP1,YY1			1 hit	TMPRSS2	intronic

c

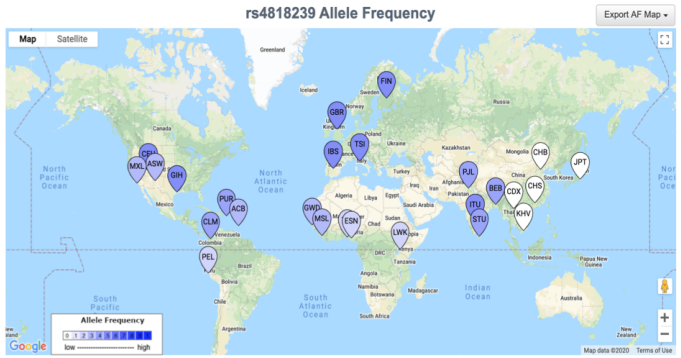

d

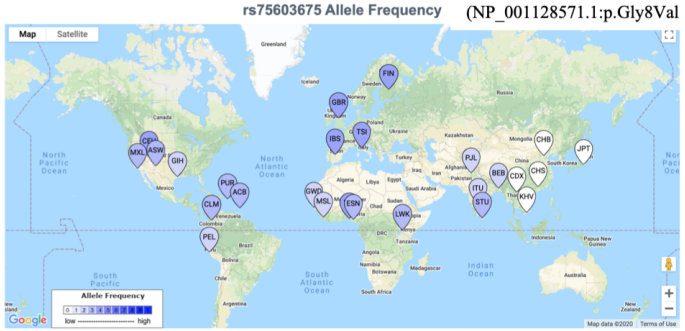

e

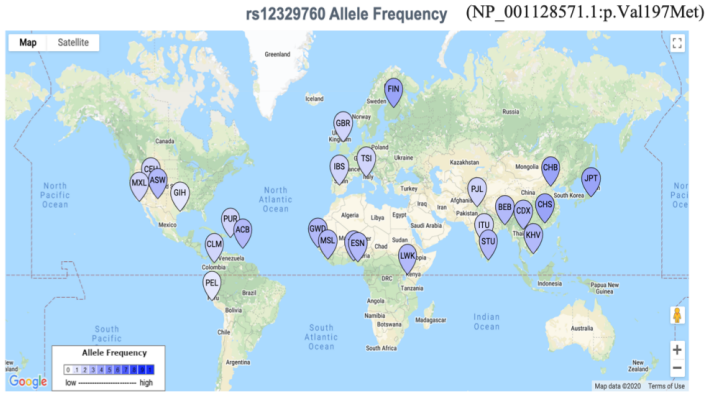

Figure S9

A.

```
                    G8V
TMPS2-2     MPPAPPGGESGCEERGAAGHIEHSRYLSLLDAVDNSKMALNSGSPPAIGPYYENHGYQPE    60
TMPS2-1     ------------------------------------MALNSGSPPAIGPYYENHGYQPE    23
                                                ***********************

TMPS2-2     NPYPAQPTVVPTVYEVHPAQYYPSPVPQYAPRVLTQASNPVVCTQPKSPSGTVCTSKTKK   120
TMPS2-1     NPYPAQPTVVPTVYEVHPAQYYPSPVPQYAPRVLTQASNPVVCTQPKSPSGTVCTSKTKK    83
            ************************************************************

TMPS2-2     ALCITLTLGTFLVGAALAAGLLWKFMGSKCSNSGIECDSSGTCINPSNWCDGVSHCPGGE   180
TMPS2-1     ALCITLTLGTFLVGAALAAGLLWKFMGSKCSNSGIECDSSGTCINPSNWCDGVSHCPGGE   143
            ************************************************************
                    V160M  V197M
TMPS2-2     DENRCVRLYGPNFILQVYSSQRKSWHPVCQDDWNENYGRAACRDMGYKNNFYSSQGIVDD   240
TMPS2-1     DENRCVRLYGPNFILQVYSSQRKSWHPVCQDDWNENYGRAACRDMGYKNNFYSSQGIVDD   203
            ************************************************************

TMPS2-2     SGSTSFMKLNTSAGNVDIYKKLYHSDACSSKAVVSLRCIACGVNLNSSRQSRIVGGESAL   300
TMPS2-1     SGSTSFMKLNTSAGNVDIYKKLYHSDACSSKAVVSLRCIACGVNLNSSRQSRIVGGESAL   263
            ************************************************************

TMPS2-2     PGAWPWQVSLHVQNVHVCGGSIITPEWIVTAAHCVEKPLNNPWHWTAFAGILRQSFMFYG   360
TMPS2-1     PGAWPWQVSLHVQNVHVCGGSIITPEWIVTAAHCVEKPLNNPWHWTAFAGILRQSFMFYG   323
            ************************************************************

TMPS2-2     AGYQVEKVISHPNYDSKTKNNDIALMKLQKPLTFNDLVKPVCLPNPGMMLQPEQLCWISG   420
TMPS2-1     AGYQVEKVISHPNYDSKTKNNDIALMKLQKPLTFNDLVKPVCLPNPGMMLQPEQLCWISG   383
            ************************************************************

TMPS2-2     WGATEEKGKTSEVLNAAKVLLIETQRCNSRYVYDNLITPAMICAGFLQGNVDSCQGDSGG   480
TMPS2-1     WGATEEKGKTSEVLNAAKVLLIETQRCNSRYVYDNLITPAMICAGFLQGNVDSCQGDSGG   443
            ************************************************************

TMPS2-2     PLVTSKNNIWWLIGDTSWGSGCAKAYRPGVYGNVMVFTDWIYRQMRADG  529
TMPS2-1     PLVTSKNNIWWLIGDTSWGSGCAKAYRPGVYGNVMVFTDWIYRQMRADG  492
            ************************************************
```

B.

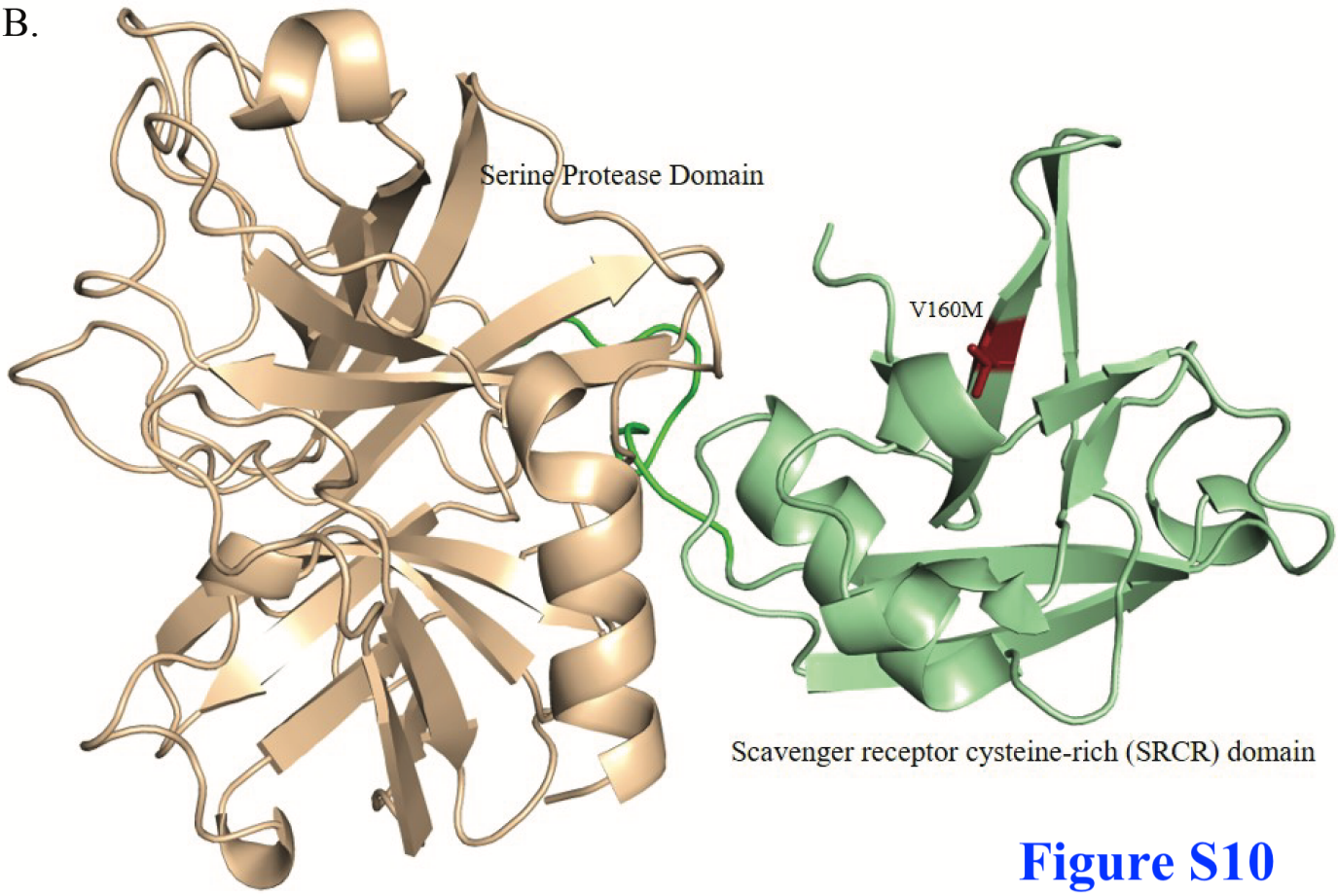

Figure S10

A1

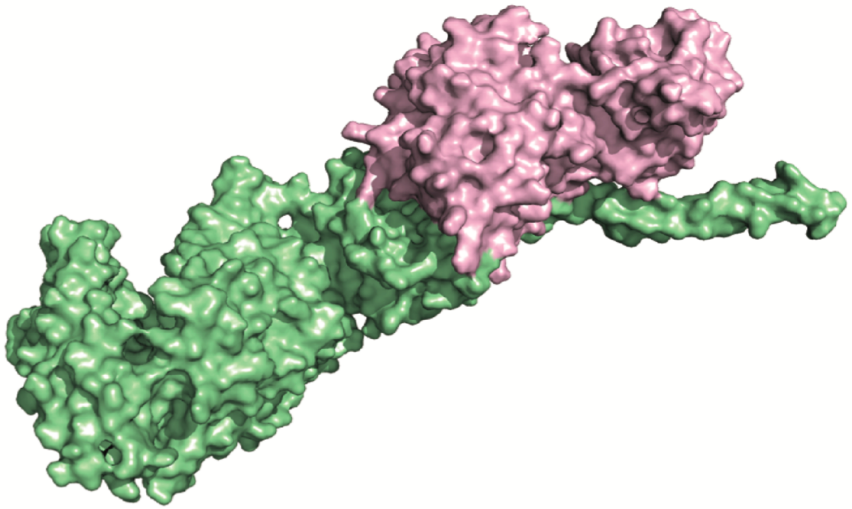

A2

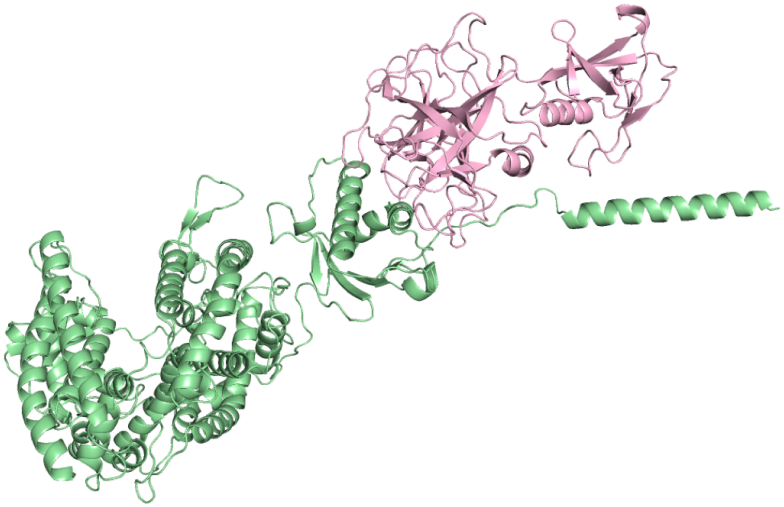

B1

B2

C

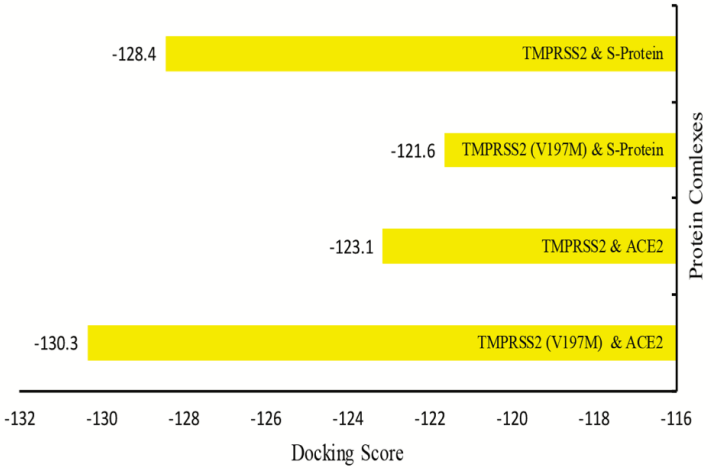

Figure S11

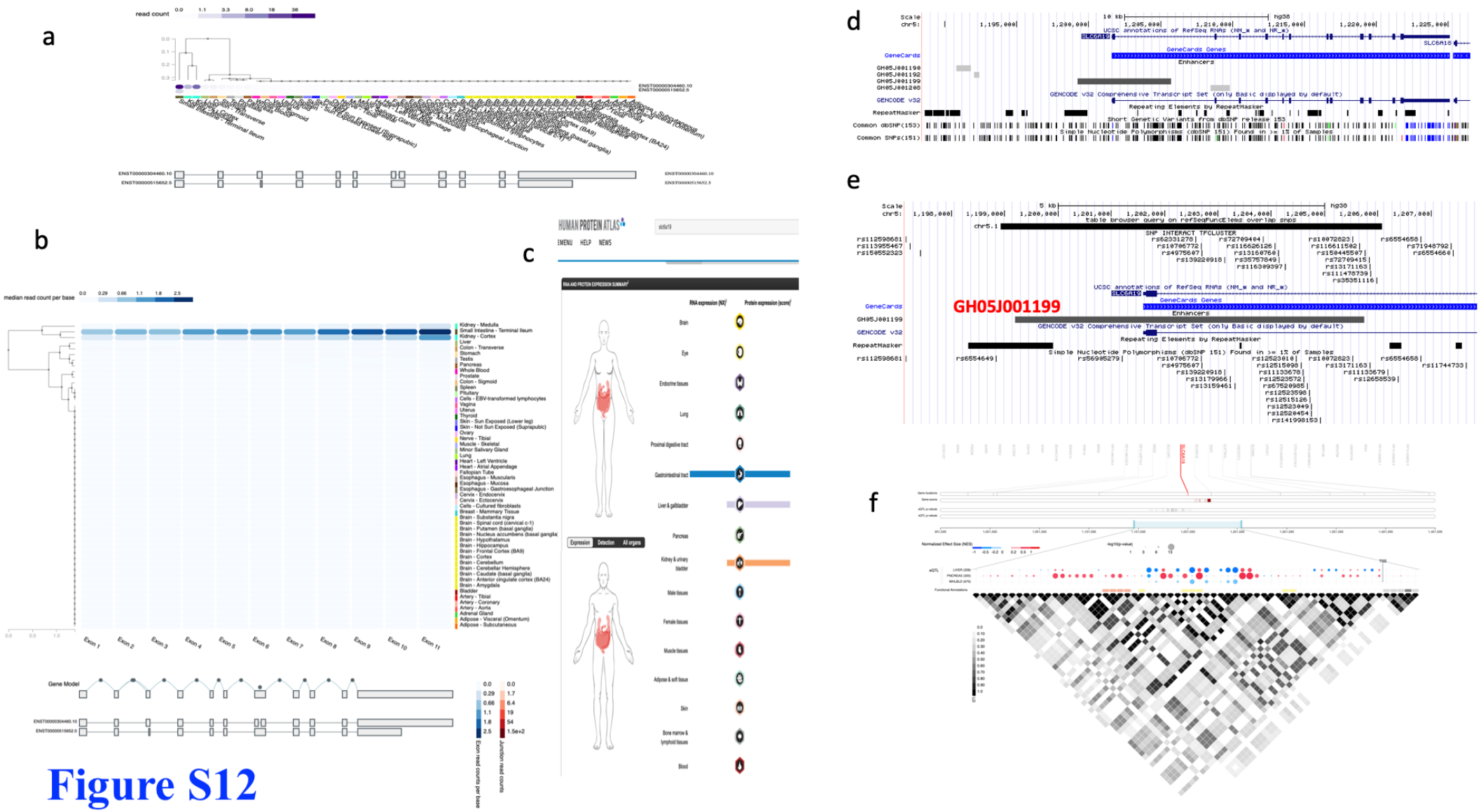
a
read count
b
median read count per base
Exon 1
Exon 2
Exon 3
Exon 4
Exon 5
Exon 6
Exon 7
Exon 8
Exon 9
Exon 10
Exon 11
Gene Model
Exon read counts per base
Junction read counts
c
HUMAN PROTEIN ATLAS
RNA expression
Protein expression
d
GH05J001199
GH05J001190
GH05J001192
GH05J001200
GeneCards
GENCODE v32
RepeatMasker
Common dbSNP(153)
Common SNPs(151)
e
GH05J001199
GeneCards
GENCODE v32
RepeatMasker
f

Figure S12

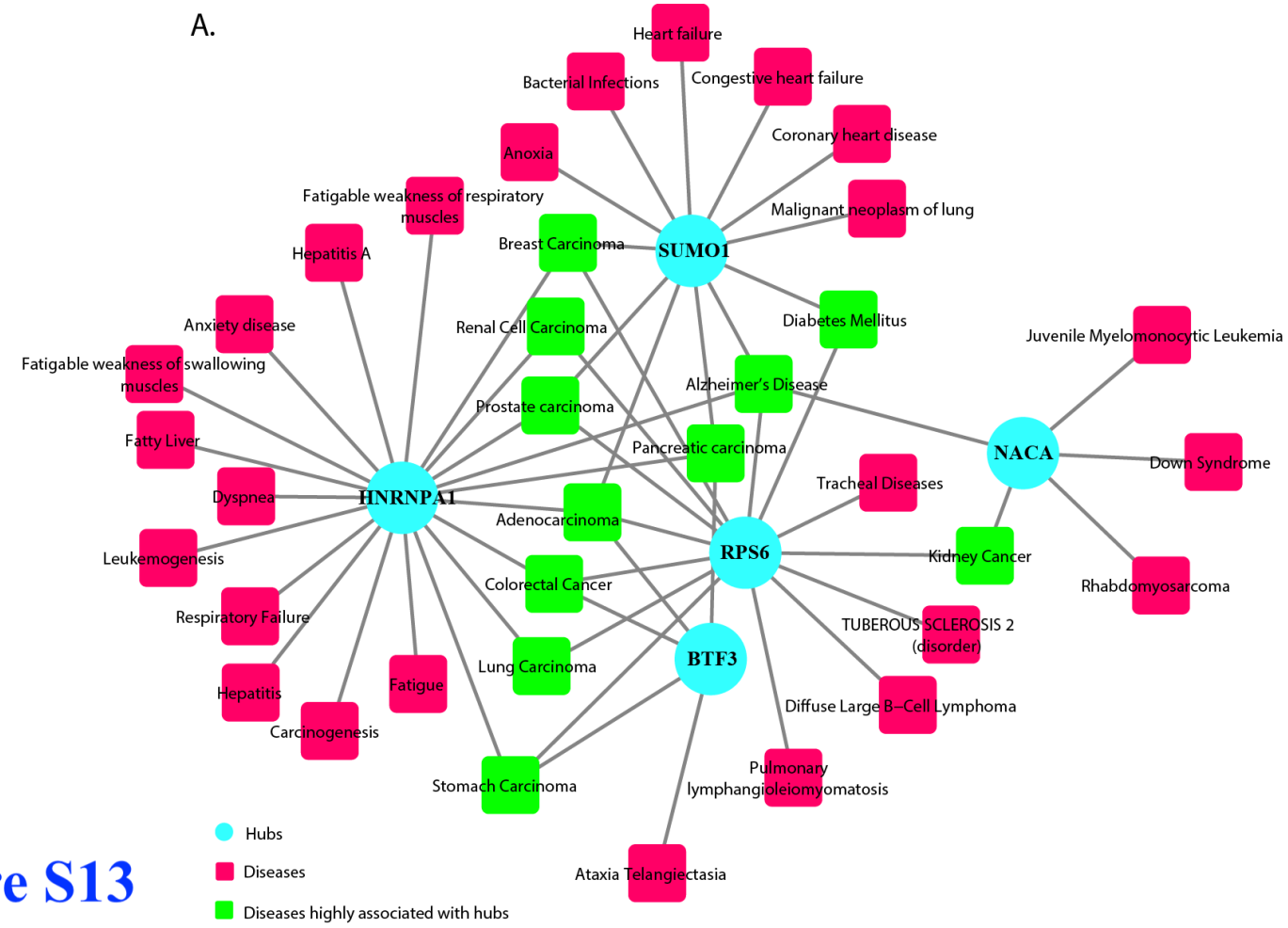
A.
Heart failure
Bacterial Infections
Congestive heart failure
Coronary heart disease
Anoxia
Malignant neoplasm of lung
Fatigable weakness of respiratory muscles
Hepatitis A
Breast Carcinoma
SUMO1
Anxiety disease
Renal Cell Carcinoma
Diabetes Mellitus
Fatigable weakness of swallowing muscles
Alzheimer's Disease
Prostate carcinoma
Fatty Liver
Pancreatic carcinoma
Dyspnea
HNRNPA1
Adenocarcinoma
Leukemogenesis
RPS6
Colorectal Cancer
Respiratory Failure
Lung Carcinoma
BTF3
Hepatitis
Fatigue
Carcinogenesis
Stomach Carcinoma
Ataxia Telangiectasia
Pulmonary lymphangioleiomyomatosis
Diffuse Large B–Cell Lymphoma
TUBEROUS SCLEROSIS 2 (disorder)
Kidney Cancer
Tracheal Diseases
NACA
Juvenile Myelomonocytic Leukemia
Down Syndrome
Rhabdomyosarcoma
Hubs
Diseases
Diseases highly associated with hubs

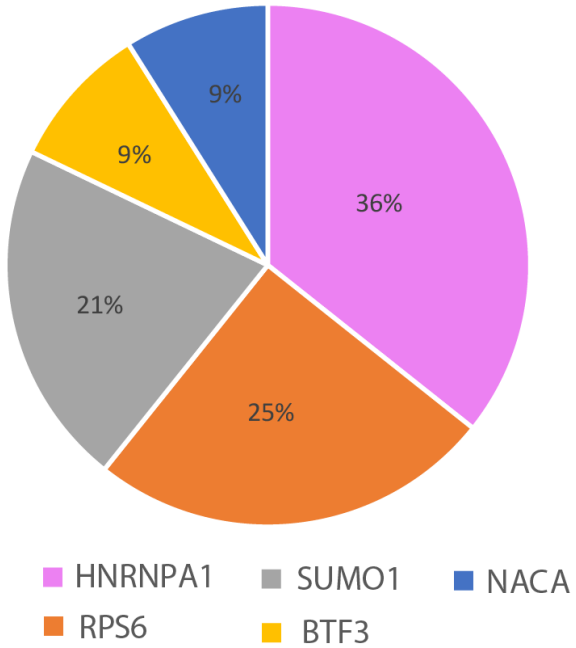
B.
36%
25%
21%
9%
9%
HNRNPA1
SUMO1
NACA
RPS6
BTF3

Figure S13

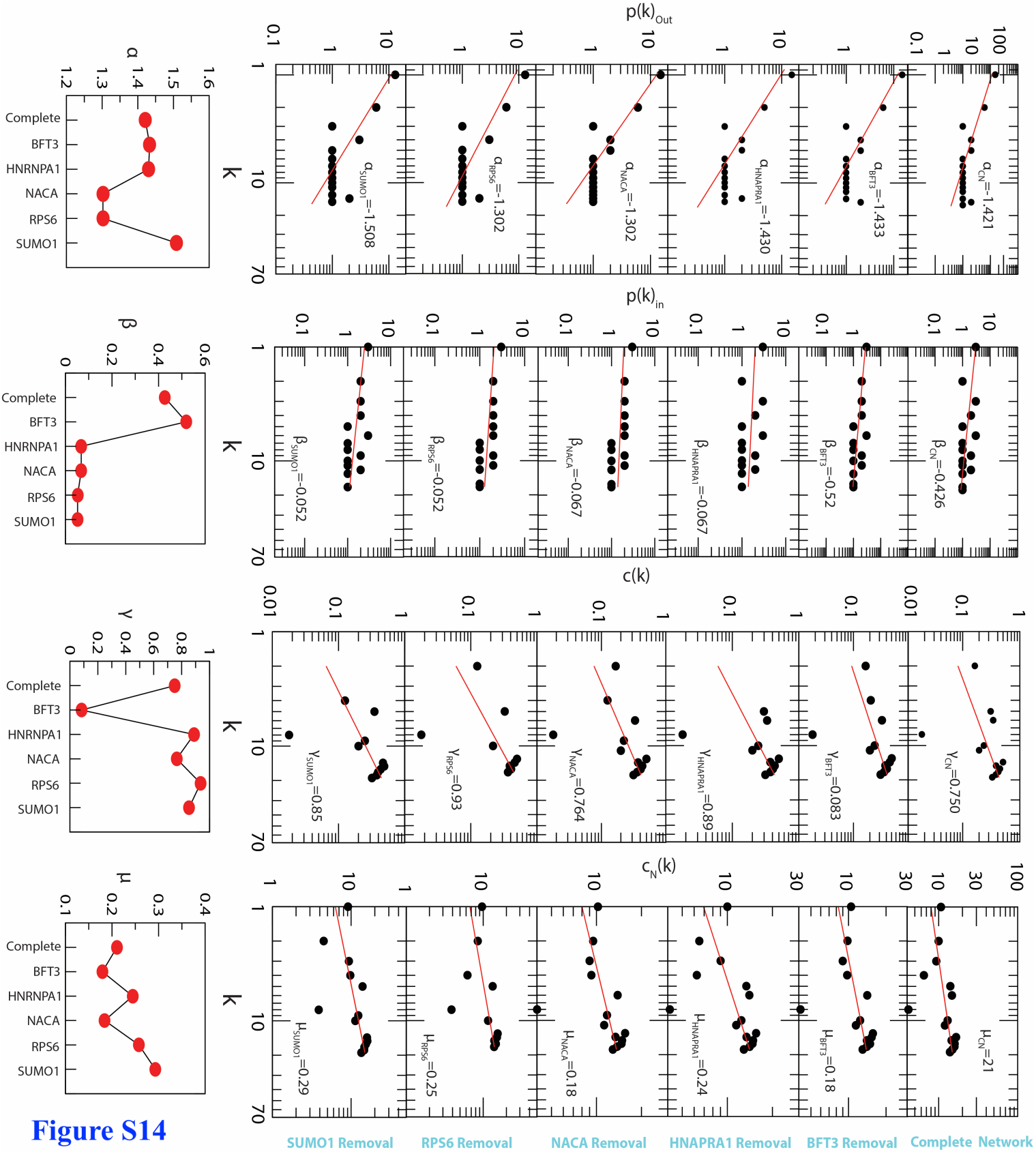
p(k)Out
αCN=-1.421
αBFT3=-1.433
αHNAPRA1=-1.430
αNACA=-1.302
αRPS6=-1.302
αSUMO1=-1.508
p(k)in
βCN=-0.426
βBFT3=-0.52
βHNAPRA1=-0.067
βNACA=-0.067
βRPS6=-0.052
βSUMO1=-0.052
c(k)
γCN=0.750
γBFT3=0.083
γHNAPRA1=0.89
γNACA=0.764
γRPS6=0.93
γSUMO1=0.85
cN(k)
μCN=21
μBFT3=0.18
μHNAPRA1=0.24
μNACA=0.18
μRPS6=0.25
μSUMO1=0.29
k
α
β
γ
μ
Complete
BFT3
HNRNPA1
NACA
RPS6
SUMO1
SUMO1 Removal
RPS6 Removal
NACA Removal
HNAPRA1 Removal
BFT3 Removal
Complete Network

Figure S14